biomolecules

MDPI

Review

Single-Cell and Spatial Transcriptomics Decode Tumor-Microenvironment Crosstalk in Colorectal Cancer Metastasis

Xize Tang †, Chaoyue Zhang †, Qianwen Wang, Jingping Yuan and Honglin Yan *

Department of Pathology, Renmin Hospital of Wuhan University, Wuhan 430060, China; 2023305231020@whu.edu.cn (X.T.); 2023305231007@whu.edu.cn (C.Z.); qwen0806@163.com (Q.W.); yuanjingping@whu.edu.cn (J.Y.)
* Correspondence: honglin@whu.edu.cn
† These authors contributed equally to this work.

Abstract

Metastasis remains the principal cause of death in colorectal cancer (CRC), and accumulating evidence indicates that it is not a tumor-autonomous process. Dissemination and organ-specific colonization of the liver, lung, and peritoneum are governed by continuous, bidirectional crosstalk between malignant cells and the cellular and extracellular compartments of the tumor microenvironment (TME). Deciphering this crosstalk requires knowing not only which cell states are present but also where they reside and with whom they interact. Single-cell RNA sequencing (scRNA-seq) resolves cellular heterogeneity at single-cell resolution but requires tissue dissociation, which erases in situ spatial information; spatial transcriptomics (ST) restores that dimension by mapping gene expression on intact sections and, with deconvolution algorithms, anchoring scRNA-seq-defined subpopulations back to their native coordinates. Organized around the metastatic cascade of local initiation, circulatory dissemination, and distant colonization, this review examines how the combined application of the two technologies has clarified tumor–microenvironment crosstalk at each stage. At the primary site, cancer stem cell heterogeneity, epithelial–mesenchymal transition (EMT) plasticity, and reciprocal signaling between budding cells and cancer-associated fibroblasts at the invasive front jointly determine invasive capacity and organotropism. During dissemination, we consider the clonal origins and transcriptional phenotypes of circulating tumor cells (CTCs) and the clustering and immune-evasion programs that enable their survival under shear stress and immune surveillance. At the metastatic site, we address multilayered remodeling of the immune contexture, fibroblast activation, extracellular matrix organization, vascular structure, and metabolic programs, emphasizing how macrophages, fibroblasts, endothelial cells, and extracellular vesicles jointly construct an immunosuppressive niche permissive to colonization. Together, these findings frame organ-specific metastasis as the spatially coordinated co-evolution of tumor cells with tissue-resident immune and stromal populations, and highlight microenvironment-directed therapeutic opportunities and spatially informed prognostic biomarkers for precision oncology.

Keywords: single-cell RNA sequencing; spatial transcriptomics; colorectal cancer; tumor-microenvironment crosstalk; organ-specific metastasis; metastatic niche remodeling; prognostic biomarkers

Check for updates

Academic Editors: Claudia Sabato and Fabio Di Domenico

Received: 30 September 2026
Revised: 5 November 2026
Accepted: 16 November 2026
Published: 18 November 2026

Copyright: © 2026 by the authors. Licensee MDPI, Basel, Switzerland. This article is an open access article distributed under the terms and conditions of the Creative Commons Attribution (CC BY) license.

1. Introduction

Colorectal cancer (CRC) is one of the malignant tumors with the highest incidence and mortality rates worldwide [1]. Although early diagnosis and comprehensive treatment strategies have substantially improved patient outcomes, metastasis remains the main cause of treatment failure and patient death. Once distant metastases occur in the liver, lungs, peritoneum, or other sites, patients often enter an advanced stage, with limited treatment options and a sharp decline in the 5-year survival rate [2]. Therefore, systematically elucidating the cellular and molecular mechanisms underlying CRC metastasis is essential for overcoming current diagnostic and therapeutic bottlenecks and achieving precise intervention; it is also of considerable clinical importance and research urgency.

For many years, bulk RNA sequencing of tissue samples has been the mainstream technology for investigating the molecular characteristics of cancer metastasis [3]. However, this technology measures the average gene-expression signal across all cells in a tissue and cannot distinguish the specific contributions of different populations, such as tumor cells, immune cells, and stromal cells. Metastasis is a complex and dynamic process involving tumor cells, circulatory dissemination, immune evasion, and microenvironmental remodeling. Because of its inherent "tissue-averaging" limitation, bulk sequencing has difficulty capturing rare metastasis-driving cell populations such as circulating tumor cells and cancer stem cells, resolving highly heterogeneous cellular states and their trajectories, or accurately characterizing the intricate cellular-interaction networks between tumor cells and the microenvironment [4]. These technical limitations have greatly restricted a deep understanding of the complete metastatic cascade.

The emergence of single-cell RNA sequencing (scRNA-seq) marked a technological revolution from the "population" level to the "individual-cell" level. By performing high-resolution transcriptomic analysis of individual cells, scRNA-seq successfully overcomes the technical gap inherent in bulk sequencing. It can unbiasedly resolve the cellular landscape within tumors [5], precisely identify cancer-cell subpopulations with metastatic potential that exhibit stem-cell-like or epithelial–mesenchymal transition (EMT) states, trace clonal evolution and lineage relationships among tumor cells, and systematically characterize the composition, functional states, and dynamic changes of diverse immune and stromal cell populations in the tumor microenvironment (TME) [6]. It therefore provides an unprecedentedly powerful tool for three-dimensional analysis of the continuous process of tumor metastasis at the single-cell level.

However, the experimental process of tissue dissociation inevitably disrupts the native spatial arrangement of cells. As a result, it is difficult to determine the in situ distribution of key tumor subpopulations in primary lesions and at invasive fronts, and it is impossible to directly reconstruct the native communication patterns among tumor, stromal, and immune cells. Spatial transcriptomics (ST) has emerged as a complementary technology to address this limitation [7]. By performing in situ sequencing on intact tissue sections, ST generates whole-section gene-expression maps while preserving tissue architecture [8]. In combination with deconvolution algorithms based on single-cell reference atlases, it can also resolve the cellular composition of individual tissue locations with high precision [9]. This approach anchors high-risk metastatic cell subpopulations identified by scRNA-seq to their original tumor locations and restores the spatial dimension lost during single-cell analysis. This review aims to synthesize how the combined application of scRNA-seq and ST has reshaped our understanding of tumor-microenvironment crosstalk during CRC metastasis. Following the classical metastatic cascade of "metastatic initiation-circulatory dissemination-distant colonization," we focus on how malignant cells engage in reciprocal signaling with the immune, stromal, vascular, and metabolic compartments of their microenvironment at each stage: how cancer stem cell heterogeneity and EMT plasticity are conditioned by and

act upon local cues at the primary site; how circulating tumor cells withstand mechanical and immunological constraints during dissemination; and how immune-cell exclusion and exhaustion, fibroblast activation, extracellular matrix reorganization, vascular remodeling, and metabolic reprogramming are coordinated to permit colonization of the liver, lung, and peritoneum. We integrate recent findings from combined single-cell and spatial analyses to delineate the spatial organization, in situ interaction mechanisms, and microenvironmental regulatory networks of key metastatic subpopulations, thereby completing a mechanistic interpretation that spans molecular features, cellular neighborhoods, and tissue-level ecology. By framing these findings as a continuous tumor-microenvironment dialogue rather than a tumor-autonomous program, this review also considers their therapeutic implications-including microenvironment-directed combination strategies and spatially informed biomarkers-and provides a reference for the precision management of metastatic CRC.

2. Overview of scRNA-Seq and ST

2.1. Overview of scRNA-Seq

Compared with bulk sequencing, scRNA-seq offers single-cell resolution and has thus become a core tool for investigating tumor heterogeneity and the regulatory mechanisms of CRC metastasis [10]. To provide a basis for understanding its application in metastasis research and the logic underlying data generation and analysis, this section briefly introduces the core principles of scRNA-seq and systematically outlines its standardized experimental and analytical workflow.

The technical core of scRNA-seq centers on the precise isolation of individual cells and the efficient, uniform amplification of low-input mRNA. Through high-throughput sequencing and bioinformatic analysis, the full transcriptomic profile of each cell is generated. The overall workflow can be summarized as a series of sequential steps: single-cell isolation, mRNA capture and reverse transcription (RT), complementary DNA (cDNA) amplification, and high-throughput sequencing (Figure 1) [11].

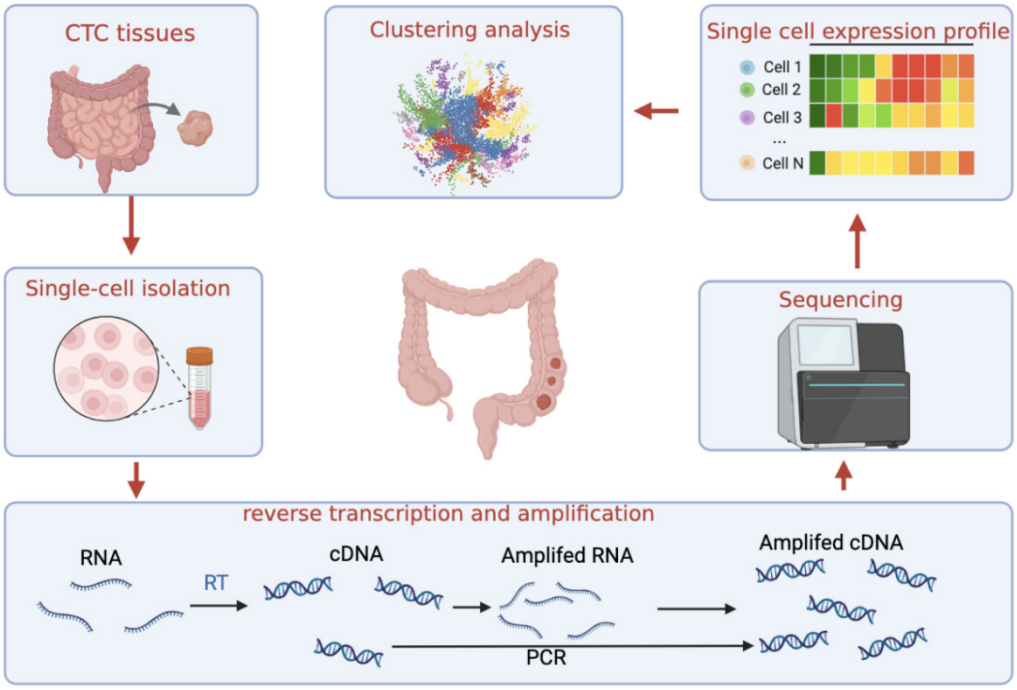


Figure 1. Typical workflow of an scRNA-seq experiment. The figure was created with BioRender.com.

2.1.1. Single-Cell Isolation and mRNA Capture

Effective single-cell isolation and high-quality capture are foundational to the scRNA-seq workflow. The technology has evolved from early low-throughput manual procedures, such as micromanipulation and fluorescence-activated cell sorting, to today's high-throughput, automated integrated platforms. The principal differences among platforms lie in their strategies for single-cell capture, mRNA labeling, and library preparation, which directly determine throughput, cost, and data quality. Currently, the major commercial platforms are based primarily on microfluidic-chip and droplet-based methods.

The Fluidigm C1 system is a representative microfluidic-chip platform [12]. Its core component is a prefabricated microfluidic chip containing hundreds of independent microreaction chambers. Through precise microfluidic control, cells from a single-cell suspension are distributed into and physically isolated within separate microchambers. Cell lysis, mRNA capture, reverse transcription, and cDNA preamplification are then completed independently in each chamber. The main advantage of this method is its high cell-capture purity, with the problem of "multiple-cell encapsulation" being almost completely avoided [13]. Because reactions occur in sealed, independent chambers, the risk of cross-contamination is low. The system is particularly suitable for studies requiring extremely high capture purity or downstream applications such as single-cell genotyping [14]. Its main limitations are relatively low throughput, with a typical yield of 96 or 800 cells per run, high chip cost, and limited flexibility.

The 10× Genomics Chromium platform is currently the most widely used droplet-based platform [15]. In a microfluidic chip, single cells are co-encapsulated with gel beads in emulsion (GEM) that carry a unique molecular identifier (UMI) and a cell barcode, generating tens of thousands of droplets almost instantaneously. Each droplet ideally contains one cell and one bead, and oligo(dT) primers on the bead capture poly(A) tails so that reverse transcription occurs in situ. All cDNA from a cell therefore carries the same barcode, while UMIs correct for polymerase chain reaction (PCR)-amplification bias and allow absolute transcript quantification [16]. High throughput, automation and low per-cell cost have made the platform the standard choice for large-scale atlases. Its limitations are a low rate of multiple-cell encapsulation, stringent requirements for cell viability and concentration, and the dependence of detectable genes on sequencing depth; shallow libraries recover fewer genes per cell, which limits how finely rare or transcriptionally similar subpopulations can be separated.

These platforms make it possible to sample primary tumors, metastatic lesions and peripheral blood within a single study, which is what allows transcriptional states to be compared across sites rather than within one tissue.

2.1.2. Reverse Transcription

After cell lysis releases mRNA, reverse transcription converts it into more stable complementary DNA (cDNA), which is then preamplified to provide sufficient template for library preparation and sequencing [17]. The efficiency and fidelity of this step directly affect downstream data quality. Its central principle is the use of oligo(dT) primers to specifically bind the poly(A) tails of mRNAs, followed by synthesis of the first cDNA strand by reverse transcriptase. To improve capture of full-length transcripts, most current technologies use a template-switching (TS) mechanism. The reverse transcriptase adds non-templated cytosine residues to the 3′ end of the cDNA, allowing complementary pairing with a template-switching oligonucleotide (TSO) containing guanine residues. The TSO sequence is thereby introduced at the 5′ end of the cDNA, ensuring that only full-length transcripts are efficiently amplified [18].

In recent years, RT technologies have continued to evolve in pursuit of higher sensitivity and efficiency. FLASH-seq combines reverse transcription and preamplification in a single-tube reaction [19] and uses the highly active SuperScript IV reverse transcriptase, substantially reducing hands-on time and completing high-sensitivity full-length library preparation in approximately 4.5 h. For studies requiring precise characterization of transcript isoforms, third-generation sequencing technologies such as HIT-scISOseq [20] optimize reverse transcription and tandem cDNA-library preparation to achieve high-throughput, high-precision full-length transcript assembly and isoform identification. In particular, to address the severe RNA degradation and incomplete poly(A) tails found in clinical archival samples, snRandom-seq uses random primers for reverse transcription and eliminates dependence on poly(A) tails [21]. It is therefore especially suitable for highly degraded archival samples, including formalin-fixed, paraffin-embedded (FFPE) tissues, and can capture transcriptome-wide information, including non-polyadenylated RNAs.

2.1.3. cDNA Amplification

Single-cell RT products are usually at the nanogram scale and must undergo in vitro amplification to yield sufficient template for sequencing. Conventional workflows rely on PCR preamplification, but early technologies were prone to amplification bias and GC-content bias [22]. Quartz-Seq2, an early yet highly influential representative technology [23], established a foundation for subsequent technological development through its poly(A)-tagging strategy. In this method, terminal deoxynucleotidyl transferase (TdT) adds a poly(A) tail to the 3′ end of the first cDNA strand, after which a primer containing poly(dT) is used to synthesize the second strand, enabling PCR amplification of full-length transcripts. This mechanism substantially improves UMI conversion efficiency, reaching 30–50%, and allows more genes to be detected with a limited amount of sequencing data. It remains an important benchmark for evaluating amplification efficiency [24].

Building on this foundation, technological advances over the past three years have focused primarily on simplifying workflows and reducing bias. In terms of workflow optimization, LAST-seq uses a distinctive linear isothermal-amplification strategy to amplify single-stranded RNA directly, bypassing reverse transcription and cDNA synthesis. This not only greatly simplifies the workflow but also provides high single-molecule capture efficiency and substantially reduces background noise [25]. Smart-seq3xpress builds on Smart-seq3 [26] by miniaturizing the reaction system and optimizing the enzyme combination. It enables direct transposase (Tn5) fragmentation and adapter ligation while reducing the number of preamplification cycles, thereby balancing high sensitivity with low cost [27]. To reduce amplification bias, GEM-X optimizes the microfluidic chip [28] and performs reverse transcription and cDNA amplification in smaller water-in-oil GEM droplets. This not only improves cell-capture efficiency but also reduces amplification bias through more efficient enzymatic reactions [29].

2.1.4. Sequencing Library Construction and Sequencing

Library construction fragments amplified cDNA, ligates sequencing adapters and sequences the resulting libraries; the reads are then filtered, aligned and clustered into subpopulations for differential expression analysis [30]. Technological evolution has moved along three lines, from short-read to long-read sequencing, from ex vivo sequencing to in situ imaging, and from manual operation to high-throughput automation. Illumina short-read sequencing [31] remains dominant but cannot resolve full-length isoforms; Oxford Nanopore [32] and PacBio HiFi [33] address this gap, and concatenation-based strategies such as Kinnex [34] have improved the cost and throughput of full-length single-cell sequencing. In parallel, imaging-based platforms such as 10× Xenium [35] and MER-

SCOPE [36] now detect thousands of panel genes at subcellular resolution, anchoring expression profiles within tissue architecture. Transposase-mediated library preparation, for example, CBTi-seq with barcoded Tn5 [37], shortens workflows and reduces amplification bias, while automated workstations (e.g., Singleron Tensor) and combinatorial indexing such as UDA-seq enable closed, low-cost, multi-omic profiling of millions of cells [38].

2.2. Overview of ST

Although scRNA-seq can resolve transcriptional heterogeneity at single-cell resolution, its central limitation is the inevitable loss of the original spatial position of cells during preparation of the single-cell suspension. Tumor initiation, progression, invasion, and metastasis are not isolated events; rather, they are coordinately regulated in three-dimensional space by multiple factors in the TME, including immune-cell infiltration, stromal remodeling, and angiogenesis. Therefore, scRNA-seq data alone are often insufficient to reconstruct spatial interactions among cells and their role in driving metastatic behavior in CRC.

ST emerged in this context. By preserving the original tissue morphology, it enables in situ capture and visualization of gene expression and directly links transcriptomic information to histopathological features [39].

ST has developed along two routes, NGS-based capture and imaging-based detection, which differ in principle and in the questions they answer. NGS platforms such as 10× Visium and BGI Stereo-seq capture mRNA on spatial-barcode arrays and sequence the resulting libraries, giving whole-transcriptome coverage, although resolution is limited by spot size. Imaging platforms such as multiplexed error-robust fluorescence in situ hybridization (MERFISH), 10× Xenium and CosMx single-molecule imaging (SMI) detect RNA directly at subcellular resolution, but only for a targeted gene panel. The two are complementary, with the former suited to panoramic discovery and the latter to precise localization and validation. Because Visium-based capture has the most mature workflow for integration with scRNA-seq, this section focuses on its experimental and analytical steps (Figure 2).

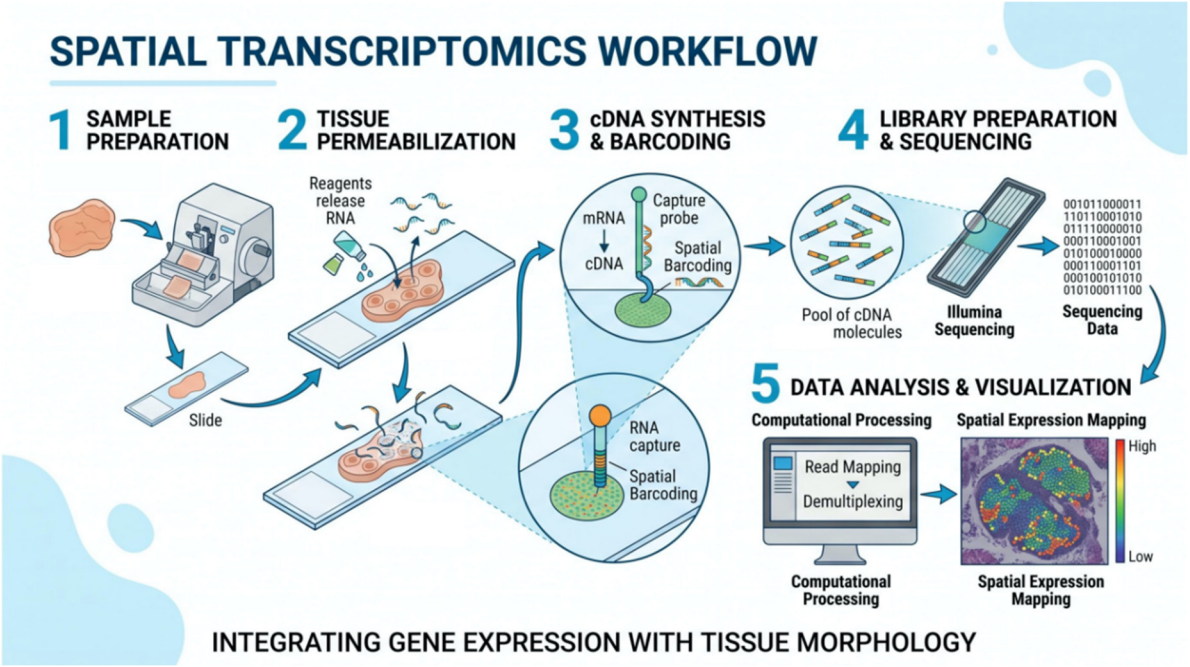


Figure 2. Typical workflow of spatial transcriptomics. The figure was generated with the assistance of PicDoc AI.

2.2.1. Tissue Preparation and Imaging

Tissue preparation is a particularly important step in the spatial transcriptomics workflow. Sample quality directly determines the final spatial resolution and gene-detection sensitivity. Fresh-frozen or formalin-fixed, paraffin-embedded (FFPE) tissue is sectioned into thin slices, usually 5–10 μm thick, which are precisely mounted onto specialized slides pre-coated with spatially barcoded capture probes [40]. After sectioning, the tissue must be immediately fixed and subjected to hematoxylin–eosin or immunofluorescence staining, followed by whole-section imaging with a high-resolution microscope. This imaging step is critical. The resulting morphological image serves as the "base map" onto which gene-expression measurements are later mapped to spatial coordinates, while also providing a visual basis for directly linking molecular features to pathological morphology.

Different platforms have different sample requirements. Among the major NGS-based platforms, 10× Genomics Visium is the most widely used commercial solution. Its capture area contains thousands of capture spots, each 55 μm in diameter with a center-to-center spacing of 100 μm. Each spot contains millions of oligonucleotide probes carrying unique spatial barcodes. The platform is compatible with both fresh-frozen and FFPE samples, although fresh-frozen samples generally require high RNA integrity, typically an RIN of at least 7. For severely degraded FFPE samples, specialized probe-hybridization capture methods are required. These methods use probes designed to target specific genes rather than relying on poly(A)-tail capture, thereby addressing RNA fragmentation [41].

Stereo-seq has reduced capture units to 500 nm through random-barcode DNA-nanoball arrays, enabling whole-transcriptome capture at subcellular resolution over a capture area of centimetres, and it can acquire morphology images and transcriptomic data from the same section [42]. 10× Genomics has since introduced Visium HD, which replaces the 55-μm spots of conventional Visium with gap-free 2 × 2 μm bins; each slide contains about 11 million capture units and supports FFPE and fresh-frozen samples, with 8 × 8 μm typically used as the initial binning unit [43]. Together, these platforms extend NGS-based ST from tissue compartments to subcellular structures, with nominal resolutions of about 2 μm for Visium HD and 500 nm for Stereo-seq.

2.2.2. Tissue Permeabilization and mRNA Capture

After the tissue section is mounted on the capture slide, permeabilization is performed to disrupt cell membranes and release intracellular mRNA molecules, allowing them to diffuse vertically and bind to spatially barcoded capture probes on the slide surface [44]. This step is critical to experimental success. The central challenge is balancing "release efficiency" with "morphological preservation": insufficient permeabilization leads to inadequate mRNA release and low capture efficiency, whereas excessive permeabilization causes excessive lateral diffusion of mRNA molecules, compromises the accuracy of their original spatial positions, and may damage tissue morphology. Therefore, before the formal experiment, a permeabilization-time gradient optimization experiment must be performed. The optimal time window is determined by jointly evaluating the intensity of fluorescently labeled cDNA signals and the integrity of tissue morphology.

In the 10× Genomics Visium workflow, for example, the 3′ end of each capture probe contains an oligo(dT) sequence that specifically binds the poly(A) tail of mRNA. This anchors the mRNA near the capture spot corresponding to its original spatial location immediately after in situ release [45]. This "capture-and-anchoring" mechanism is central to preserving spatial fidelity. For probe-based capture of FFPE samples, the method does not depend on poly(A) tails. Instead, a pair of probes is designed to hybridize to adjacent sequences on the same mRNA molecule. An amplifiable template is generated only when

both probes bind as a pair and are ligated, thereby greatly improving detection specificity and reducing background noise.

2.2.3. Reverse Transcription and Spatial-Barcode Labeling

After mRNA capture, RT is performed in situ on the slide. The RT primer is complementary to a specific sequence on the capture probe and uses the captured mRNA as a template to synthesize the first cDNA strand. The distinctive feature of this process is that each synthesized cDNA molecule inherits the unique spatial barcode and unique molecular identifier carried by the capture spot where it is located. The spatial barcode records the precise two-dimensional coordinate of the tissue section from which the transcript originated, while the UMI corrects for subsequent PCR-amplification bias and enables absolute transcript quantification [46]. This "in situ spatial-barcode labeling" strategy is the fundamental technical feature that distinguishes ST from scRNA-seq and ensures that every sequencing read generated downstream can be traced back to its original spatial coordinate.

After RT, spatially barcoded cDNA is eluted from the slide and transferred to a tube for subsequent processing. For special sample types requiring whole-transcriptome coverage, such as severely degraded FFPE samples, ST platforms based on random-primer strategies can be used. Random-primer RT eliminates dependence on poly(A) tails and enables comprehensive capture of noncoding RNAs and degraded fragments. Representative platforms include imRandom-seq [47] and Stereo-seq V2 [48]. The former integrates the entire workflow, including in situ RT, into a microfluidic chip and enables automated, standardized spatial capture of total RNA from FFPE sections. The latter achieves single-cell-resolution spatial mapping of total RNA in FFPE sections. These two routes, the conventional poly(A)-dependent workflow and the random-primer-based whole-transcriptome strategy, are complementary and together expand the range of sample types suitable for ST.

2.2.4. Library Preparation, Sequencing, and Data Analysis

The eluted cDNA undergoes standard procedures, including second-strand synthesis, end repair, A-tailing, sequencing-adapter ligation, and PCR enrichment, to generate high-throughput sequencing libraries compatible with platforms such as Illumina. After passing library quality control, the libraries are sequenced, typically in paired-end mode: one read records the spatial-barcode and UMI sequences, while the other reads the inserted gene fragment. After quality control and filtering of the raw sequencing data, gene-expression measurements are mapped to the corresponding spatial coordinates in the tissue image using spatial-barcode information, generating a spatial gene-expression matrix [49].

Data analysis is the key stage at which ST delivers its value. The core workflow includes spatial alignment and registration of the tissue image with gene-expression data, unsupervised clustering based on the expression matrix, identification of spatially variable genes, and mapping of cell-type annotations onto the tissue architecture. In recent years, integrated analytical strategies have become an important area of progress. Through deconvolution algorithms or probabilistic models, scRNA-seq data from the same tissue type or from public databases can be mapped onto each capture spot in the spatial-transcriptomic dataset. This preserves spatial information while inferring the cellular composition and relative proportions of each spot. The strategy compensates for the limitations of NGS-based ST in single-cell resolution and enables researchers to investigate cell–cell communication in situ, track the frontiers of tumor-clone evolution, and depict the spatial dynamics of immune-cell infiltration [50].

2.3. Inherent Limitations of scRNA-Seq and ST

Neither technology is unbiased, and their limitations are as complementary as their strengths. For scRNA-seq, enzymatic dissociation removes cells from their neighbours and selectively loses fragile populations such as hepatocytes and some stromal cells, while inducing stress-response programs that were not present in situ. Spatial context is lost by definition. Shallow 3′ libraries capture transcript ends and detect fewer genes from lowly expressed programs, so weakly transcribed regulators and isoform-level information are under-represented. Doublets, ambient RNA and cell-calling thresholds also influence which subpopulations appear at all. For ST, resolution and throughput trade off against each other. Spot-based platforms average several cells per capture unit, so cell-type composition has to be inferred by deconvolution rather than measured directly, whereas high-resolution platforms multiply the number of units to be sequenced and analyzed. Capture efficiency is lower than for dissociated cells, RNA integrity constrains what can be recovered from archival tissue, and probe-based panels interrogate only a predefined transcript set. Both approaches remain expensive, sensitive to batch effects, and dependent on analytical choices such as the integration method, the clustering resolution and the reference atlas, each of which can change the answer. Their findings are therefore correlative, and the studies reviewed below are best read as hypothesis-generating unless supported by functional perturbation. Where possible, the two technologies are used together precisely because each compensates for the blind spots of the other.

3. Applications of scRNA-Seq and ST in Dissecting CRC Metastasis Mechanisms

Metastasis proceeds through heterogeneous evolution of the primary tumor, circulatory dissemination and colonization of distant organs, and at each stage malignant cells exchange signals with the immune, stromal, vascular and metabolic compartments around them. These interactions are local, transient and cell-type specific, which is why they are difficult to resolve with bulk approaches and why the two technologies described above are used together here. Using CRC as a model of organ-specific metastasis, this section follows that sequence and asks how crosstalk at each stage shapes organ tropism and the outcome of colonization.

3.1. Heterogeneity of the Primary Tumor and Early Metastatic Initiation

The initiation of CRC metastasis is an early event that occurs within the primary tumor and depends on coordinated interactions among several cell types. Recent single-cell and spatial work has resolved these interactions in situ and shifted attention from the properties of individual malignant cells to the signals they exchange with their neighbours. Four themes recur in this literature, namely cancer-stem-cell heterogeneity, EMT-state plasticity, regulation at the invasive front, and the single-cell and spatial organization that distinguishes primary from metastatic niches (Figure 3, Table 1).

3.1.1. Cancer Stem Cell (CSC) Subpopulations: An Intrinsic Cellular Basis for Metastatic Initiation

CSCs are a central cell population involved in CRC development, invasion, metastasis, and postoperative recurrence. Lin et al. profiled 26 specimens from 18 patients with primary or liver-metastatic CRC by 10× Chromium scRNA-seq and retained 111,224 cells after quality control (median 1389 genes per cell). In that dataset, classical CSC marker genes were not expressed by one discrete population; instead, they were diffusely distributed across stem/transcriptional-amplifying and immature epithelial states [51]. Clustering based on high CSC-feature scores revealed substantial interindividual heterogeneity among CSCs

from different patients. This complex heterogeneity could not be explained by a single marker gene.

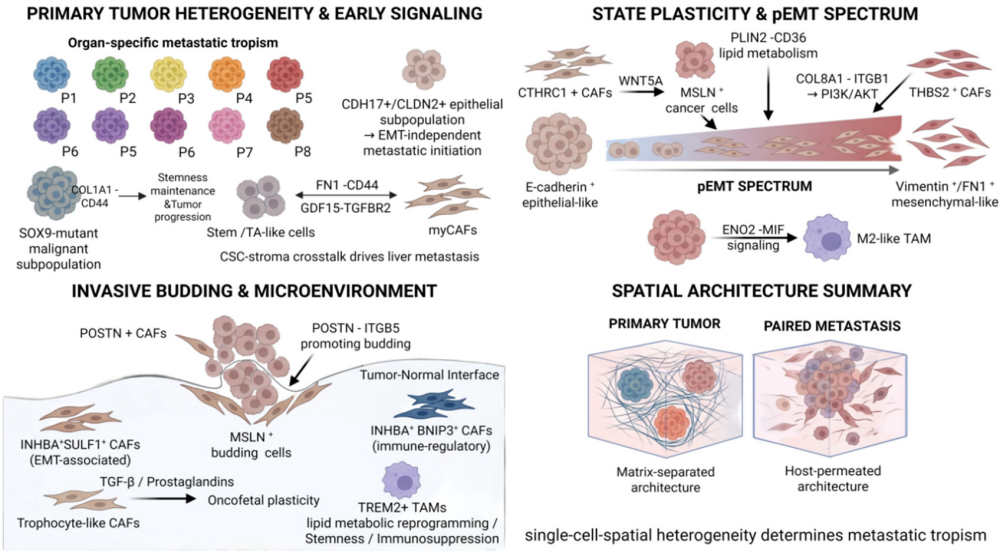


Figure 3. Heterogeneity of the primary tumor and early metastatic initiation. Integrated single-cell and spatial transcriptomic view of metastatic initiation in CRC. The four panels show CSC-like subpopulation heterogeneity and CSC-stroma crosstalk (**top left**), the partial-EMT spectrum with its CAF- and metabolism-derived inputs (**top right**), invasive-front budding and the oncofetal niche (**bottom left**), and matrix-separated versus host-permeated spatial architectures (**bottom right**). Figure was created with BioRender.com.

Table 1. Mechanisms underlying primary-tumor heterogeneity and early metastatic initiation.

Category	Research Topic	Key Finding	Technical Core	Clinical Significance	References
Cancer-stem-cell heterogeneity	Broad expression of CSC markers and patient heterogeneity	CSCs' marker genes are broadly distributed across multiple epithelial cell states (stem/transcriptional-amplifying and immature epithelium), and CSCs from different patients show substantial interindividual heterogeneity	scRNA-seq	Shows that CSC heterogeneity cannot be explained by a single marker gene; CSC-targeted therapy may need to be individualized	[51]
	Organ-specific metastatic tropism of CSC subpopulations	Eight CSC subpopulations (P1–P8) were identified; P1/P2 were enriched in ovarian metastases, whereas P3/P4 were specifically enriched in liver metastases	scRNA-seq + ST	Confirms that CSC heterogeneity is the cellular basis of organ-specific metastasis	[52]
	Stem/TA-like cell–myCAF interactions drive liver metastasis	Stem/TA-like cells interact with myCAFs through FN1–CD44 and GDF15–TGFBR2 and drive liver metastasis	scRNA-seq + ST	Shows that CSC–stromal-cell crosstalk is a key driver of liver metastasis	[53]
	EMT-independent metastatic-initiating cell state	IKKα loss stabilizes tight junctions and expands a CDH17^{+}/CLDN2^{+} epithelial subpopulation that dominates metastases	scRNA-seq	Challenges the traditional view that EMT is the only route to metastasis	[54]
	SOX9-mutation-driven maintenance of stemness and microenvironmental remodeling	The SOX9-mutant malignant epithelial subpopulation (Scissor^{+}) shows enhanced stemness; the COL1A1–CD44 axis mediates stemness maintenance	scRNA-seq + TCGA mutation data	Directly links a specific gene mutation to a CSC functional phenotype at single-cell resolution	[55]

Table 1. *Cont.*

Category	Research Topic	Key Finding	Technical Core	Clinical Significance	References
EMT-state plasticity	pEMT states determine tropism for liver versus peritoneal metastasis	Cancer cells in liver metastases exhibit epithelial-like pEMT, whereas those in peritoneal metastases exhibit mesenchymal-like pEMT; differentiated pEMT states determine organ tropism	scRNA-seq	Monitoring pEMT states may predict the metastatic organ	[56]
	EMT-feature-driven molecular subtyping and prognosis	Across five integrated single-cell cohorts, the aggressive C3 subtype showed pronounced EMT activation, associated with high metastatic potential and poor prognosis	Multi-cohort scRNA-seq integration	EMT-feature-based molecular subtyping may guide prognostic assessment	[57]
	The ENO2–MIF axis drives M2 polarization and liver metastasis	$ENO2^+$ cancer cells drive M2 macrophage polarization through MIF signaling; ENO2–MIF inhibition reduces liver metastasis	scRNA-seq + ST + mouse models	Indicates the therapeutic potential of targeting the ENO2–MIF axis to block EMT	[58]
	$APOE^+$ macrophages induce EMT through TNFSF12	$APOE^+$ macrophages induce EMT-like changes through TNFSF12/TNFRSF12A signaling; FOSL2 transcriptionally activates TNFRSF12A	scRNA-seq	Expands the recognized role of immune cells in regulating EMT	[59]
	Continuous trajectory from malignant epithelial cells to CAFs	Malignant epithelial cells transition through $CXCL1^+$ intermediate cells to $SFRP2^+$ CAFs, mainly at the invasive front	scRNA-seq + ST	Provides evidence that cancer cells can directly transform into CAFs through EMT	[60]
	$CTHRC1^+$ CAFs drive EMT through WNT5A–MSLN	$CTHRC1^+$ CAFs secrete WNT5A, which targets the MSLN receptor, drives EMT in epithelial cells, and enhances invasion	scRNA-seq + ST	Identifies a new pro-metastatic CAF population and its ligand–receptor target	[61]
	$THBS2^+$ CAFs mediate chemotherapy resistance through COL8A1	$THBS2^+$ CAFs secrete COL8A1, which binds ITGB1, activates PI3K/AKT, and drives EMT, resulting in oxaliplatin resistance	scRNA-seq	Reveals a new mechanism of CAF-mediated chemotherapy resistance	[62]
	PLIN2 links lipid metabolism and EMT through CD36	PLIN2 promotes EMT through a CD36-dependent pathway and regulates TAM polarization toward the M2 phenotype	scRNA-seq + multi-omics	Links lipid metabolism with EMT and the immunosuppressive microenvironment	[63]
	ATRX loss accelerates EMT through chromatin plasticity	ATRX loss reduces HNF4A chromatin accessibility, releases lineage-differentiation constraints, and accelerates EMT and metastasis	scRNA-seq + epigenetic analysis	Reveals a key role for chromatin remodeling in metastasis	[64]
	CiPDOs capture the OnFS state and identify AP-1 regulation	The chemically induced organoid model captures an OnFS cell population and identifies AP-1 as a key regulator maintaining the OnFS state	scRNA-seq + organoid model	Provides a new experimental platform for studying plastic evolution and chemotherapy resistance	[65]
	KLF7 induces EMT through TGF-β as a PMS biomarker	KLF7 marks the PMS1 subtype and induces EMT through autocrine TGF-β signaling; EGCG can inhibit KLF7 transcriptional activity	scRNA-seq + multi-omics	Proposes KLF7 as a therapeutic target and EGCG as a candidate drug	[66]

Table 1. *Cont.*

Category	Research Topic	Key Finding	Technical Core	Clinical Significance	References
Invasive front and in situ interactions	Interactions between MSLN$^+$ budding cells and POSTN$^+$ CAFs	MSLN$^+$ budding-potential cells were identified at the invasive front; POSTN$^+$ fibroblasts promote tumor budding through POSTN–ITGB5 interactions	scRNA-seq + spatial analysis	Directly links a cancer-cell population and CAF subtype to tumor-budding morphology	[67]
	Spatial division of labor among INHBA$^+$ CAFs promotes metastasis	Two INHBA$^+$ CAF populations localize to the invasive front: INHBA$^+$SULF1$^+$ CAFs promote EMT, whereas INHBA$^+$BNIP3$^+$ CAFs are immunomodulatory	scRNA-seq + Xenium spatial localization	Shows that CAFs cooperatively promote metastasis through spatial division of labor at the same invasive front	[68]
	Panoramic map of epithelial–fibroblast interactions	An integrated map reveals how cellular heterogeneity, developmental trajectories, and communication shape spatial niches	scRNA-seq + ST	Provides a panoramic reference for understanding the functional organization of the invasive front	[69]
	Oncofetal plasticity at the invasive front of early CRC	Oncofetal plasticity is already widespread at the invasive front in T1-stage cancer and is induced by trophocyte-like CAFs through TGF-β and prostaglandins	scRNA-seq + high-resolution ST	Moves the apparent acquisition of metastatic potential to a much earlier stage and emphasizes very early intervention	[70]
Single-cell spatial heterogeneity of the metastatic niche	Conserved lactate-consuming metabolic niches in primary and metastatic lesions	spFBA was developed and identified lactate-consuming metabolic niches in both primary and metastatic lesions	ST + spFBA metabolic model	Provides a theoretical basis for therapies targeting metabolic adaptation	[71]
	Stromal segregation in primary lesions versus host infiltration in metastatic lesions	Primary lesions show stromal segregation, whereas liver metastases show host infiltration, with tumor cells embedded in the liver's immune and vascular framework	scRNA-seq + ST	Clarifies spatial differences between primary and metastatic lesions and supports differentiated treatment strategies	[72]
	Immunosuppressive role of TREM2$^+$ lipid-loaded TAMs in liver metastasis	TREM2$^+$ lipid-loaded TAMs are specifically enriched in liver metastases, localize to the invasive margin, recruit neutrophils through ALOX5/ALOX5AP, and promote stemness	CyTOF + scRNA-seq + ST + lipidomics	Identifies TREM2$^+$ TAMs as a liver-metastasis target; depletion may enhance anti-PD-1 efficacy	[73]

Integrated analysis of single-cell and ST can further clarify the association between heterogeneous CSCs and organ-specific metastatic tropism. Li et al. identified a heterogeneous population of CSC-like cells in primary CRC lesions by integrating scRNA-seq with ST. Based on their transcriptional features, these cells could be divided into eight subpopulations, P1–P8 [52]. Spatial localization and functional validation showed that P1 and P2 were enriched in primary lesions and ovarian metastases, whereas P3 and P4 were specifically concentrated in primary lesions and liver metastases. These findings directly demonstrate, at the level of cellular subpopulations, that CRC heterogeneity is an important basis for organ-specific metastasis. Zhan et al. addressed a different side of the same question. Instead of asking which organ a stem-like subpopulation favors, they asked what keeps it in that state, and found that stem/TA-like cells and myofibroblast-like cancer-associated fibroblasts (myCAFs) in primary and liver metastatic tumors communicate through FN1-CD44 and GDF15-TGFBR2, a circuit proposed to form a positive feedback loop that drives liver metastasis and is associated with recurrence after chemotherapy [53].

Recent work has also revealed noncanonical regulatory pathways governing the intrinsic state of CSCs, broadening the understanding of the origins of CSC heterogeneity. Alvarez-Villanueva et al. found that loss of IKKα promoted expansion of a $CDH17^+/CLDN2^+$ epithelial subpopulation by stabilizing tight-junction components. This subpopulation predominated in metastatic lesions, and disruption of CLDN2 completely eliminated the metastatic advantage conferred by IKKα loss [54]. The finding revealed a metastatic-initiating cell state that does not depend on EMT and challenged the traditional view that EMT is the only route to metastasis. Notably, these cells lacked LGR5 and other canonical intestinal stem-cell markers. This indicates that metastatic capacity does not necessarily depend on conventional proliferative, stem-like cells. Instead, metastatic CRC may be initiated by non-stem cells that acquire stem-like functional programs. This finding expanded the conceptual boundaries of metastatic-cell origins from a complementary perspective.

At the molecular level of CSC-maintenance mechanisms, Pan et al. integrated scRNA-seq data from 23 CRC samples with The Cancer Genome Atlas (TCGA) mutation data and identified a SOX9-mutation-associated malignant epithelial subpopulation known as Scissor+ [55]. This population exhibited enhanced stemness features, and the COL1A1-CD44 axis was markedly upregulated in SOX9-mutant tumors. Immunohistochemistry and mouse xenograft models confirmed that the COL1A1-CD44 axis mediates SOX9-mutation-driven maintenance of stemness and tumor progression, directly linking a specific gene mutation to a CSC functional phenotype at single-cell resolution.

3.1.2. Plasticity of the EMT State: A Core Functional Program of Tumor Invasion and Migration

The acquisition of metastatic potential depends not only on the heterogeneity of CSC subpopulations but also on the state plasticity of cancer cells. Single-cell studies have shown that EMT is not a binary on/off state but a continuous and highly plastic spectrum of partial-EMT (pEMT) states. Specific states within this spectrum influence organ-specific metastasis and are precisely regulated by the tumor microenvironment. Yu et al. performed scRNA-seq analysis of samples from primary CRC lesions, liver metastases, and peritoneal metastases [56]. Cancer cells in colorectal liver metastases (CRLM) exhibited an epithelial-like pEMT state, with high expression of epithelial markers such as E-cadherin and only limited activation of mesenchymal-related genes. By contrast, cancer cells in colorectal peritoneal metastases (CRPM) displayed a mesenchymal-like pEMT state, with high expression of mesenchymal markers such as vimentin and FN1, enabling adaptation to the microenvironment of free survival and implantation within the peritoneal cavity. These findings demonstrate that, before liver or peritoneal metastasis develops, cancer cells in the primary tumor have already undergone distinct pEMT-state differentiation. Differences in these states may constitute an intrinsic reason why primary CRC exhibits different patterns of organ tropism. A more recent study integrating five single-cell cohorts further supports this view. Based on vascular endothelial growth factor receptor-positive ($VEGFR^+$) tumor-cell features, the study divided patients with CRC into distinct subtypes and found that the aggressive C3 subtype exhibited pronounced EMT activation, which was closely associated with high metastatic potential and poor prognosis [57].

More recent applications of single-cell technologies have further revealed how interactions between tumor cells and microenvironmental cells actively drive transitions between EMT states. $ENO2^+$ cancer cells were significantly enriched in liver metastases. ENO2 directly bound MIF and inhibited its CHIP-mediated ubiquitin degradation, thereby activating the MIF signaling pathway, promoting tumor-cell-macrophage interactions, and driving the polarization of macrophages toward the M2 phenotype. ST confirmed the colocalization of $ENO2^+$ cancer cells and M2 macrophages in metastatic lesions. ENO2 knockout

significantly inhibited tumor growth and liver metastasis in mouse models, whereas the ENO2-MIF inhibitor pyrithioxin effectively reduced the metastatic burden. These findings revealed the therapeutic potential of targeting tumor-immune interactions to block EMT [58]. In addition to cancer-associated fibroblasts (CAFs) and tumor cells themselves, tumor-associated macrophages can also drive EMT by directly secreting signaling molecules. $APOE^+$ macrophages secrete TNFSF12, which acts on $TNFRSF12A^+$ tumor cells, activates BCL2L1-related survival signaling, and induces EMT-like changes. FOSL2 directly transcriptionally activates TNFRSF12A. Clinical analysis showed that combined high expression of TNFSF12 and TNFRSF12A was significantly associated with advanced disease and poorer survival, further expanding the recognized role of immune cells in regulating EMT [59].

The dynamic progression of EMT is not completed autonomously by cancer cells. Instead, it depends on active signals from multiple cell types in the tumor microenvironment, with CAFs playing a particularly important regulatory role. Yang et al. used single-cell transcriptomic analysis to resolve a continuous transcriptional trajectory from malignant epithelial cells toward CAFs: malignant epithelial cells first transitioned into $CXCL1^+$ intermediate cells and subsequently differentiated into $SFRP2^+$ CAFs [60]. This finding provides molecular evidence that cancer cells can directly transform into CAFs through an EMT program. In situ localization using ST showed that this state transition occurred mainly at the tumor invasive front, indicating that it is an important in situ event during metastatic initiation. Further studies have shown that CAFs secrete multiple key signaling molecules and thereby establish a complex regulatory network that promotes EMT. Lu et al. used this to identify a new prometastatic CAF population, $CTHRC1^+$ CAFs [61]. This population secretes WNT5A, which binds to the MSLN receptor on neighboring cancer cells and drives epithelial cells to undergo EMT, thereby enhancing their invasive capacity. In addition to this paracrine mechanism, CAFs can influence EMT through other pathways. Factors secreted by tumor cells themselves, such as SPP1 and SEMA3C, can also independently induce EMT. CAF heterogeneity is closely linked to chemotherapy resistance as well. One study showed that $THBS2^+$ CAFs in CRC secrete COL8A1, which binds to the ITGB1 receptor on drug-resistant tumor cells, activates the PI3K/AKT pathway, and continuously drives EMT, ultimately leading to oxaliplatin resistance [62].

EMT plasticity also intersects extensively with cellular metabolic reprogramming and epigenetic regulation. By integrating multi-omics analyses, Yang et al. found that the lipid-droplet-associated protein PLIN2 promotes EMT through a CD36-dependent pathway while also regulating the polarization of tumor-associated macrophages (TAMs) toward the M2 phenotype. This links lipid metabolism with EMT and the immunosuppressive microenvironment [63]. At the epigenetic level, Cammareri et al. showed that loss of the chromatin-remodeling enzyme ATRX reduces the chromatin accessibility of the transcription factor HNF4A. This releases restrictions on lineage differentiation in colonic epithelial cells, promotes their transition toward mesenchymal and other multilineage states, and is accompanied by upregulation of EMT-related genes, ultimately accelerating tumor-metastatic progression [64]. EMT-associated plasticity is also closely connected to treatment resistance. To model and investigate this plasticity in vitro, a team at Peking University developed a chemically induced patient-derived organoid model of CRC, termed chemically induced patient-derived organoids (CiPDOs). Using a culture system containing four small molecules (EGF, CHIR99021, LDN-214117, and FGF2), the model stably maintains tumor cells in an oncofetal state (OnFS) over long periods. Through scRNA-seq, the team systematically identified an OnFS cell population at single-cell resolution for the first time. These cells did not express classical intestinal stem-cell markers such as LGR5, but they activated programs including EMT and exhibited stronger migratory capacity and chemotherapy resistance. A regulatory-network model constructed from data identified the

AP-1 transcription-factor family as a key regulator maintaining the OnFS state. This work provided a new experimental platform for investigating the plastic evolution of tumor cells and its relationship with chemotherapy resistance [65]. Another study used scRNA-seq and other multi-omics data to classify premetastatic-state (PMS) cells into two subtypes, PMS1 and PMS2, and identified KLF7 as a key biomarker of the PMS1 subtype [66]. The study found that KLF7 may induce EMT by activating an autocrine transforming growth factor beta (TGF-β) signaling pathway, which may represent an important mechanism driving CRC liver metastasis. It was also found that the green-tea polyphenol EGCG can inhibit KLF7 transcriptional activity, thereby blocking TGF-β signaling and EMT. These findings suggest that EGCG may be a candidate for further investigation in CRC characterized by high KLF7 expression.

These findings illustrate that EMT heterogeneity is best interpreted as one arm of a bidirectional tumor–microenvironment dialogue: the state adopted by a cancer cell reflects the cues it receives and, in turn, constrains the microenvironmental partners it can engage.

3.1.3. The Tumor Invasive Front: A Key In Situ Functional Region for Metastatic Initiation

The invasive front at the interface between tumor and normal tissue is where metastatic initiation begins, and it is also where tumor–stroma crosstalk operates most directly. By integrating large-scale scRNA-seq data, Ma et al. identified a population of budding-potential cells with high MSLN expression at the invasive front of CRC tumors [67]. Spatial analysis showed that $POSTN^+$ fibroblasts surrounded these $MSLN^+$ cells and jointly promoted tumor budding and metastasis through interactions mediated by the POSTN-ITGB5 ligand-receptor pair. This study established a direct association, at both the single-cell molecular and spatial levels, among a specific cancer-cell subpopulation, a CAF subtype, and the morphological characteristics of tumor metastasis.

scRNA-seq identified two $INHBA^+$ CAF subpopulations: $INHBA^+SULF1^+$ CAFs, which were associated with EMT features, and $INHBA^+BNIP3^+$ CAFs, which displayed an immunomodulatory phenotype. Xenium-based spatial localization showed that both $INHBA^+$ CAF populations were located in regions enriched for invasive tumor cells. $INHBA^+$ myCAFs frequently accumulated with $SPP1^+$ macrophages and promoted EMT, whereas $INHBA^+$ iCAFs were located in specialized immunosuppressive niches where they recruited regulatory T cells. These findings reveal, within the same invasive-front region, a finely organized pattern in which CAFs promote metastatic initiation through spatial division of labor and coordinated activity [68]. In addition, integrated analyses have systematically mapped epithelial-fibroblast interactions. They have shown how cellular heterogeneity, developmental trajectories, and intercellular communication shape tumor progression and spatial niches, providing a panoramic reference for understanding the functional organization of the invasive front at the broader level of cellular-interaction networks [69].

A recent breakthrough study combined scRNA-seq with high-resolution ST to systematically analyze T1-stage CRC samples and found that oncofetal plasticity was already widespread at the invasive front during the earliest stages of tumor formation [70]. scRNA-seq data indicated that these oncofetal states were not driven by genetic mutations intrinsic to the tumor cells. Instead, they were induced by a subpopulation of fibroblasts in the tumor microenvironment, particularly trophocyte-like cancer-associated fibroblasts, which secreted factors such as TGF-β and prostaglandins. Further demonstrated that these fibroblasts and oncofetal cells were highly colocalized at the invasive front and displayed spatial compartmentalization patterns resembling those of normal intestinal tissue. The cancer cells reactivated programs that are normally highly expressed only during embryonic development, thereby acquiring embryonic-like capacities for rapid proliferation, migration, and adaptation to the microenvironment. This study shifted the apparent timing

of metastatic-potential acquisition toward the earliest stages of tumor development and challenged the conventional view that metastasis occurs only in advanced cancer. It also emphasizes the potential importance of very early intervention in cancer treatment.

3.1.4. Single-Cell–Spatial Heterogeneity: A Microenvironmental Regulatory System for Metastatic-Niche Remodeling

Fundamental differences in cellular heterogeneity and spatial organization between primary tumors and metastatic lesions have profound effects on metastatic progression, reflecting the adaptation of disseminated cells to the resident microenvironment of a foreign tissue. Maspero et al. developed spatial flux-balance analysis (spFBA), a method that combined ST data with metabolic-network models and used flux sampling to infer the directionality and relative activity of reactions at each spatial location [71]. When applied to high-resolution spatial data from primary CRC lesions and paired liver metastases, the method identified lactate-consuming metabolic niches in both the primary and metastatic sites. This finding suggested that CRC may follow a conserved metabolic-adaptation strategy during metastasis.

Another study integrated scRNA-seq with ST to systematically reveal fundamental differences in the spatial architecture and cellular composition of primary CRC lesions and liver metastases [72]. Primary CRC generally displayed a stromal-segregation pattern: proliferatively active tumor regions were physically separated from immune-active regions by stromal interfaces rich in CAFs. Single-cell transcriptomic cell-type analysis further confirmed that tumor cells, CAFs, and immune cells in primary lesions exhibited clear regional distributions. By contrast, liver metastases displayed a host-infiltration pattern, in which tumor cells were directly embedded within the liver's native immune and vascular framework. Single-cell cell-type profiling showed extensive infiltration of myeloid cells and regulatory immune cells in metastatic lesions, forming an immunosuppressive metastatic microenvironment. This fundamental difference, determined jointly by single-cell heterogeneity and spatial tissue organization, indicates that primary and metastatic tumors should be treated with different therapeutic strategies.

The studies described above characterized spatial differences between primary and metastatic lesions at the level of tissue organization. Recent work has further validated these differences at the level of specific cell types. Wang et al. integrated cytometry by time-of-flight (CyTOF), single-cell transcriptomics, ST, and lipidomics and identified a lipid-loaded population of TREM2$^+$ TAMs that was specifically enriched in CRC liver metastases [73]. These cells highly expressed lipid-metabolism genes such as APOE, LIPA, and GPNMB and accumulated large numbers of lipid droplets intracellularly. Spatial analysis showed that these cells were primarily located at the invasive margin and within tumor-internal, colon-like luminal structures rather than being uniformly distributed throughout the metastatic lesion. This distribution pattern was consistent with the previously described feature of liver metastases, in which myeloid cells extensively infiltrate the tumor-liver interface. Functionally, TREM2$^+$ TAMs produced leukotrienes through the ALOX5/ALOX5AP pathway, recruited neutrophils, and promoted tumor-cell stemness. In vivo depletion of this population relieved immunosuppression and enhanced the efficacy of anti-programmed cell death protein 1 (PD-1) therapy. This finding translated the broad spatial differences between primary and metastatic lesions into a concrete macrophage population that is specifically enriched in liver metastases, localized to defined spatial regions, and endowed with immunosuppressive functions through lipid metabolism. It therefore provides a specific cellular and molecular example for understanding the differences between the microenvironments of the two types of lesions.

3.2. Circulating Tumor Cells (CTCs) and Distant Tumor Dissemination

Circulating tumor cells (CTCs) are a key population of cancer cells that detach from primary or metastatic lesions, enter the bloodstream, and mediate hematogenous metastasis. Tumor cells may passively detach as a result of vascular injury and/or actively invade the circulatory system through EMT, thereby forming CTCs. However, only a very small fraction of CTCs can survive the shear stress of blood flow and immune surveillance and initiate early colonization [74]. Although CTCs are extremely rare in peripheral blood, they serve as a direct "liquid vehicle" for systemic tumor dissemination and play a central role in CRC metastasis to the liver and lungs [75]. scRNA-seq and spatial-transcriptomic analyses can resolve their clonal origins, molecular heterogeneity, mechanisms of survival in the circulation, and directional metastatic features at single-cell resolution (Figure 4, Table 2) [76].

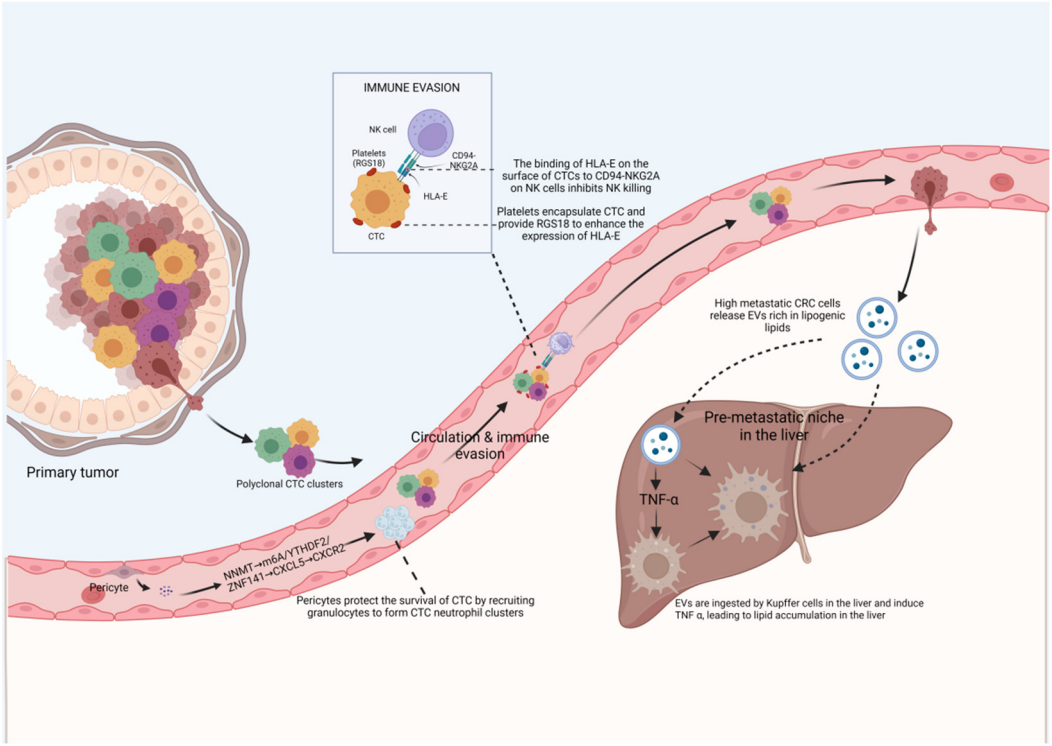


Figure 4. CTCs and distant tumor dissemination. Polyclonal CTC clusters intravasate from the primary tumor, evade NK-cell killing through HLA-E-CD94-NKG2A and platelet-derived RGS18, and are shielded by pericyte-driven CTC-neutrophil clusters, while lipogenic extracellular vesicles (EVs) precondition the hepatic pre-metastatic niche via Kupffer-cell TNF-α. Figure was created with BioRender.com. Colors are used only to distinguish cell types.

The metastatic potential of CTCs is not a uniform feature. Intrinsic genomic clonal differences and the continuous phenotypic spectrum of EMT form the underlying basis that determines patterns of tumor dissemination and organ-specific tropism. Single-cell genomic technologies, particularly paired single-cell whole-exome sequencing (scWES) of CTCs, primary lesions, and metastatic lesions from the same patient, are redefining metastatic mechanisms at the level of clonal origin. Studies have shown that dissemination may begin very early during tumor development and that CTCs retain the subclonal architecture of the tumor of origin. In CRC, liver metastases may arise from polyclonal CTC clusters, whose genetic heterogeneity sometimes exceeds that of the primary lesion [77]. This challenges the prevailing assumption that metastasis originates from a single dominant clone and emphasizes that clonal diversity within CTC populations is a key driver of metastatic adaptation.

Table 2. CTCs and distant tumor dissemination.

Category	Research Topic	Key Finding	Technical Core	Clinical Significance	References
CTC clonal and phenotypic heterogeneity	Polyclonal CTC dissemination and retention of subclonal architecture	Liver metastases may arise from polyclonal CTC clusters, whose genetic heterogeneity can exceed that of the primary lesion	scWES	Challenges the assumption that metastasis arises from a single dominant clone	[77]
	CTC pEMT states determine metastatic-organ tropism	Liver-directed CTCs show epithelial-like pEMT, whereas peritoneum-directed CTCs show mesenchymal-like pEMT	scRNA-seq	Noninvasive prediction of metastatic-organ tropism through scRNA-seq of peripheral-blood CTCs	[78]
CTC survival in the circulation and immune evasion	Pericytes recruit neutrophils through the m6A/YTHDF2/ZNF141 axis and CXCL5 to form CTC clusters	NNMT-high pericytes recruit neutrophils through CXCL5/CXCR2, causing neutrophil–tumor-cell aggregation and CTC-cluster formation	scRNA-seq + ST	Targeted NNMT inhibition in pericytes eliminates CTC clusters and suppresses liver metastasis	[79]
	CTCs suppress NK cells through HLA-E/CD94–NKG2A	CTC-expressed HLA-E binds CD94–NKG2A on NK cells and directly inhibits NK-cell cytotoxicity	scRNA-seq	Reveals a key molecular pathway of innate immune evasion by CTCs	[80]
	CTCs acquire RGS18 by engulfing platelets to strengthen immune evasion	CTCs acquire RGS18 from platelets, upregulate HLA-E, and enhance immune evasion	scRNA-seq	Expands the understanding of acquired immune evasion by CTCs	[81]
Target-organ microenvironment and colonization	$SPP1^+$ and $FOLR2^+$ TAMs enrich in liver metastases and create an immunosuppressive microenvironment	$SPP1^+$ and $FOLR2^+$ TAMs establish proliferative and immune-exclusion signaling axes that jointly favor CTC colonization	scRNA-seq + ST	Reveals coordinated mechanisms by which the metastatic immune microenvironment promotes CTC colonization	[82]
	$SPP1^+$ TAMs induce T-cell exhaustion through SPP1/CD44/PI3K/AKT	SPP1 promotes tumor growth through the CD44/PI3K/AKT axis and induces functional T-cell exhaustion	scRNA-seq	Clarifies the core immunosuppressive signaling pathway of $SPP1^+$ TAMs	[82]
	TGF-β induces an $SPP1^+$ macrophage phenotype and creates a dual immune barrier	TGF-β induces the $SPP1^+$ macrophage phenotype, creating a dual immune barrier	scRNA-seq	Reveals a key role for TGF-β in shaping the metastatic immune microenvironment	[83]
	CRC-cell EVs drive hepatic lipid accumulation and precondition the metastatic niche	Highly metastatic CRC cells increase fatty-acid synthesis; steatotic lipids accumulate in EVs, which are taken up by Kupffer cells and induce TNF-α secretion	Lipidomics + scRNA-seq	Shows how tumor cells remotely remodel the hepatic microenvironment through EVs to promote colonization	[84]
Multi-omics clinical translation	Synchronous scDNA + scRNA co-sequencing dynamically monitors clonal evolution	Joint single-cell DNA and RNA sequencing captures multidimensional genomic alterations and transcriptomic phenotypes	Single-cell multi-omics (DNA + RNA co-sequencing)	Provides a dynamic basis for individualized adjustment of targeted and immunotherapies	[85]

Once clonal origins have been characterized, scRNA-seq can reveal the association between CTC functional states and metastatic-organ tropism. One study found that CTCs with a propensity for liver metastasis exhibited an epithelial-like pEMT phenotype, whereas CTCs with a propensity for peritoneal metastasis exhibited a mesenchymal-like pEMT phenotype [78]. This finding links the genomic background of CTCs to their functional phenotype. Monitoring pEMT states through single-cell transcriptomic analysis of peripheral-blood CTCs may therefore enable noninvasive prediction of metastatic organ tropism before

lesions become detectable by imaging, providing a potential window for early individualized intervention.

After entering the bloodstream, CTCs must overcome both mechanical injury and immune clearance. Cluster formation and multiple immune-evasion pathways are two major supports for their long-term survival in the circulation and preservation of metastatic potential. Studies have shown that CTC-neutrophil clusters form mainly at the vascular-immune interface of primary tumors. A pericyte subpopulation with high NNMT expression upregulated CXCL5 through the m6A/YTHDF2/ZNF141 axis, thereby activating the CXCL5/CXCR2 pathway and recruiting neutrophils to aggregate with tumor cells and form CTC-neutrophil clusters [79]. Targeted inhibition of NNMT in pericytes eliminates CTC clusters and suppresses liver metastasis, identifying a potential strategy for blocking early dissemination by interfering with cluster formation. Even when cluster formation improves mechanical tolerance, circulating CTCs must establish multiple molecular pathways to evade killing by innate immune cells such as natural killer (NK) cells. Single-cell analysis has shown that CTCs express HLA-E, which binds the CD94/NKG2A receptor on NK cells and directly inhibits NK-cell cytotoxicity [80]. CTCs also acquire the RGS18 gene by engulfing platelets, thereby increasing their own HLA-E expression and strengthening immune evasion [81].

When CTCs reach target organs such as the liver, their colonization efficiency depends heavily on their ability to remodel the local microenvironment. Integrated single-cell and ST analyses have shown that CRC liver metastases were enriched for two specialized TAM populations, $SPP1^+$ TAMs and $FOLR2^+$ TAMs. These populations established proliferative and immune-exclusion signaling axes, respectively, and jointly created an immunosuppressive microenvironment favorable to CTC colonization [82]. $SPP1^+$ TAMs were particularly important: through the SPP1/CD44 pathway, they activated PI3K/AKT signaling to promote tumor growth and drove T cells toward functional exhaustion, suppressing antitumor immunity at multiple levels. TGF-β could induce this inhibitory $SPP1^+$ macrophage phenotype, thereby creating a dual immune barrier [83]. Another study combining lipidomics and found that extracellular vesicles (EVs) secreted by highly metastatic CRC cells precondition the metastatic niche by promoting lipid accumulation in the liver [84]. Mechanistically, highly metastatic CRC cells increased fatty-acid synthesis, leading to an increase in lipids that promoted steatosis within EVs. These EVs were predominantly taken up by hepatic Kupffer cells, inducing TNF-α secretion and further aggravating hepatic lipid accumulation. Inhibiting fatty-acid synthesis in CRC cells reduces hepatic lipid accumulation and lowers the incidence of liver metastasis. This work showed how CRC cells remotely remodel the hepatic microenvironment through EVs, creating conditions that facilitate CTC colonization after arrival in the liver. It also broadens the understanding of CTC-mediated metastasis: metastatic capacity depends not only on intrinsic CTC properties but also on preconditioning of the target-organ microenvironment by primary tumor cells through EVs.

With the development of single-cell multi-omics, CTC research has moved beyond enumeration toward functional classification and precision medicine. Daniel et al. reported that simultaneous single-cell DNA and RNA co-sequencing of CTCs could capture genomic alterations, such as driver mutations and copy-number changes, together with transcriptomic phenotypes, such as EMT state, stem-cell features, and drug-target expression. This enables dynamic monitoring of clonal evolution during treatment and provides an important basis for individualized adjustment of targeted and immunotherapies [85].

3.3. Colonization of Metastatic Lesions and Remodeling of the Tumor Microenvironment

Successful colonization is the step at which disseminated tumor cells and the microenvironment of a distant organ interact bidirectionally, remodel one another, and establish a

new lesion. Whether arriving cells are cleared by local immune surveillance or succeed in establishing overt metastases depends on how the resident cell populations of the target organ are reshaped. scRNA-seq and ST provide analytical capabilities spanning cellular atlases, molecular mechanisms, and spatial interaction networks, and have become central to resolving how the colonization-permissive niche is assembled (Figure 5, Table 3).

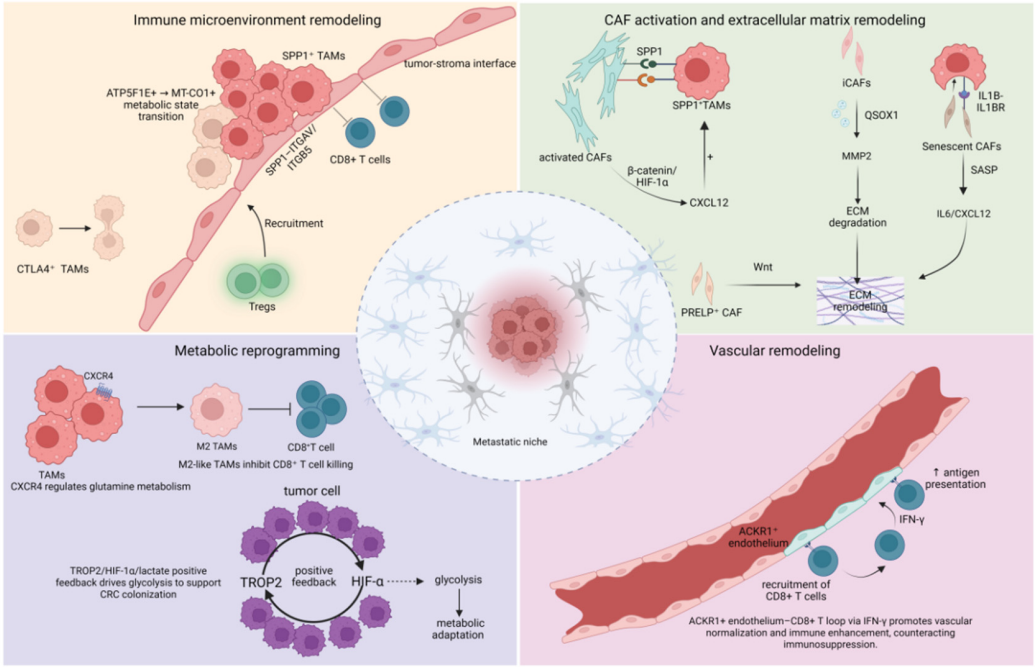


Figure 5. Colonization of metastatic lesions and remodeling of the tumor microenvironment. Four coordinated remodeling programs surround the metastatic niche: SPP1+ and CTLA4+ TAM-mediated immunosuppression, CAF-driven extracellular matrix (ECM) remodeling with the SPP1-CAF-CXCL12 feedback loop, CXCR4- and TROP2/HIF-1α-dependent metabolic reprogramming, and ACKR1+ endothelium-mediated vascular normalization. The figure was created with BioRender.com. Colors are used only to distinguish the four panels and the cell types within them.

Table 3. Colonization of Metastatic Lesions and Remodeling of the Tumor Microenvironment.

Category	Research Topic	Key Finding	Technical Core	Clinical Significance	References
Immune-microenvironment remodeling	SPP1$^+$ TAMs are enriched in liver metastases	SPP1$^+$ TAM abundance is associated with poor prognosis	scRNA-seq	Prognostic marker and immunotherapy target	[86]
	Origin and metabolic trajectory of SPP1$^+$ TAMs	SPP1$^+$ TAMs derive mainly from peripheral-blood monocytes and switch from glycolysis to oxidative phosphorylation	scRNA-seq and trajectory analysis	Reveals functional adaptation during colonization	[87]
	CTLA4$^+$ TAMs in liver metastases	Highly proliferative and immunosuppressive CTLA4$^+$ TAMs are associated with shorter survival	scRNA-seq	Supports cooperative macrophage-mediated niche formation	[88]
	SPP1$^+$ TAMs recruit Tregs through MIF	SPP1$^+$ TAMs recruit Tregs through MIF signaling	scRNA-seq + ST	Mechanism of immunosuppression	[89]
	SPP1$^+$ TAMs promote angiogenesis	The CD44/POU2F2/BCL9L axis promotes angiogenesis	scRNA-seq	Proangiogenic TAM mechanism	[90]

Table 3. *Cont.*

Category	Research Topic	Key Finding	Technical Core	Clinical Significance	References
Fibroblast activation and ECM remodeling	CAFs shape budding cancer cells	CAFs remodel ECM and focal-adhesion signaling to drive migration	ST	Spatial role in invasion	[91]
	TAM–fibroblast niche formation	SPP1$^+$ TAMs and activated fibroblasts create a CD8$^+$ T-cell-poor, Treg-rich niche	scRNA-seq + spatial imaging	Stromal–immune regulation of growth	[92]
	SPP1–CAF–CXCL12 feedback	CRC SPP1 activates CAF β-catenin/HIF-1α and CXCL12	scRNA-seq + ST	Targetable stromal feedback	[93]
	SEMA3C–NRP2–MAPK signaling	CAF SEMA3C induces EMT and liver metastasis	scRNA-seq	Prometastatic CAF pathway	[94]
	QSOX1-rich EVs from iCAFs	QSOX1 degrades ECM through MMP2 and enables invasion	scRNA-seq + mouse model	QSOX1 inhibition reduces lung metastasis	[95]
	Senescent CAFs and chemotherapy resistance	SASP factors IL6 and CXCL12 weaken chemotherapy killing	scRNA-seq + ST	Stromal drug-resistance mechanism	[96]
Vascular remodeling	Abnormal vasculature supports immune escape	Disorganized vessels supply nutrients and create immune-privileged regions	scRNA-seq + ST	Supports vascular normalization	[97]
	ACKR1$^+$ endothelium enhances immunity	ACKR1$^+$ endothelial cells recruit CD8$^+$ T cells and enhance antigen presentation	scRNA-seq + TCR sequencing + ST	Cellular evidence for vascular normalization	[98]
Metabolic reprogramming	TAM metabolic adaptation	Fatty-acid oxidation and cholesterol synthesis support an M2-like state	scRNA-seq + ST	Metabolic control of TAM polarization	[99]
	CXCR4–glutamine metabolism	CXCR4 promotes M2 polarization; blockade enhances anti-PD-1	scRNA-seq and animal studies	Reverses immunosuppression	[100]
	TROP2/HIF-1α/lactate feedback	Feedback reinforces glycolysis and colonization	scRNA-seq and spatial multi-omics	Links metabolism to colonization	[101]
	KIAA1199-high EVs precondition liver	EVs reprogram hepatocytes and recruit neutrophils	scRNA-seq and spatial multi-omics	Systemic metabolic mechanism	[102]

3.3.1. Remodeling of the Immune Microenvironment

Within the framework of tumor-microenvironment crosstalk, the immune compartment is not a passive bystander: its composition and spatial organization are actively reshaped by incoming tumor cells and, in turn, influence whether colonization proceeds. scRNA-seq has systematically characterized the distinctive immunosuppressive features of metastatic lesions. In CRC liver metastasis, Liu et al. identified an SPP1$^+$ TAM population specifically enriched in liver metastases; its abundance was significantly associated with poor prognosis [86]. Subsequent trajectory analysis showed that these SPP1$^+$ TAMs mainly derived from peripheral-blood monocytes rather than resident Kupffer cells and underwent metabolic reprogramming from a glycolysis-biased ATP5F1E$^+$ state to an MT-CO1$^+$ state dependent on mitochondrial oxidative phosphorylation [87]. A CTLA4$^+$ TAM population with high proliferative and immunosuppressive activity was also enriched in liver metastases and associated with shorter survival [88]. ST localized SPP1$^+$ TAMs mainly to the tumor-stroma interface, where interactions such as SPP1-Itgav/Itgb5 restricted cytotoxic T-cell infiltration and induced exhaustion. SPP1$^+$ TAMs also recruited Tregs through MIF signaling [89] and promoted angiogenesis through the CD44/POU2F2/BCL9L axis [90].

3.3.2. Fibroblast Activation and Extracellular Matrix (ECM) Remodeling

CAFs are a key component of the tumor stroma and a principal cellular mediator of tumor-microenvironment crosstalk. ST showed that budding-potential cancer cells at the invasive front frequently contacted CAFs, which remodelled the ECM and regulated focal-adhesion signaling to shape cancer-cell morphology and drive migration [91]. In liver metastases, $SPP1^+$ TAMs and activated fibroblasts form spatial interactions that create a niche lacking functional $CD8^+$ T cells and enriched in Tregs [92]. CRC-derived SPP1 activated β-catenin/HIF-1α in CAFs and induced CXCL12, creating an SPP1-CAF-CXCL12 positive-feedback axis that promoted EMT and immune evasion [93]. CAF-derived SEMA3C bound NRP2 on tumor cells and activated mitogen-activated protein kinase (MAPK) to induce EMT and liver metastasis [94]. In lung metastases, inflammatory CAFs released QSOX1-rich extracellular vesicles; QSOX1 enhanced MMP2 activity and degraded ECM, enabling invasion. QSOX1 deletion or inhibition reduced lung metastasis and prolonged survival [95]. Senescent CAFs also released IL-6 and CXCL12 through senescence-associated secretory phenotype (SASP) and weakened chemotherapy-mediated tumor-cell killing [96].

3.3.3. Vascular Remodeling

The vascular endothelium of a distant organ is the first physical barrier that circulating tumor cells must cross, and it is also an active signaling interface that governs local immune accessibility. Abnormal and disorganized tumor vessels supplied nutrients, while barrier damage created local immune-privileged regions that facilitated immune escape [97]. After effective neoadjuvant therapy, $ACKR1^+$ endothelial cells recruited $CD8^+$ T cells into the tumor parenchyma and enhanced antigen presentation through interferon-γ signaling, providing cellular evidence that vascular normalization can improve immunotherapy [98].

3.3.4. Metabolic Reprogramming

Metabolic reprogramming is simultaneously a consequence and a driver of tumor-microenvironment crosstalk: competition for nutrients and the exchange of metabolites couple tumor cells to the immune and stromal compartments that surround them. In liver metastases, the microenvironment drove macrophages to increase fatty-acid oxidation and cholesterol synthesis, supporting an immunosuppressive M2-like state [99]. CXCR4-regulated glutamine metabolism promoted M2 polarization and suppressed $CD8^+$ T-cell cytotoxicity; CXCR4 blockade reversed immunosuppression and enhanced anti-PD-1 therapy [100]. CRC cells reinforced glycolysis through a TROP2/HIF-1α/lactate feedback pathway and enhanced colonization [101]. KIAA1199-high tumor cells released extracellular vesicles that reprogrammed hepatocyte metabolism and preconditioned a liver niche favorable to neutrophil recruitment [102].

4. Conclusions

This review examined the core mechanisms revealed by scRNA-seq and ST across the three key stages of the CRC metastatic cascade. In the primary tumor, cancer stem cells display substantial heterogeneity and interact with specific CAF subpopulations; these features may determine whether cancer cells metastasize to the liver or the peritoneum. Dynamic changes across the pEMT-state spectrum not only confer invasive capacity on cancer cells but also provide an intrinsic molecular basis for the selection of metastatic direction. Oncofetal plasticity at the invasive front, together with CAF-promoted EMT programs, suggests that metastatic potential may be activated at a very early stage of tumor development. Taken together, the evidence reviewed here supports a shift in emphasis from the metastatic tumor cell to the dialogue it maintains with its microenvironment—a shift that reframes both the mechanistic question and the therapeutic target.

Once cancer cells enter the circulation, CTCs disseminate as polyclonal populations, cluster with neutrophils for protection, and evade immune attack through HLA-E, adaptations that together allow them to withstand blood-flow shear stress and immune surveillance. Their transcriptional phenotypes may allow the target organ of metastasis to be predicted noninvasively. During colonization, $SPP1^+$ TAMs shift their metabolism from glycolysis toward oxidative phosphorylation and cooperate with CAFs through an SPP1-CAF-CXCL12 positive-feedback axis to construct an immunosuppressive niche. Integrated single-cell and spatial data have further resolved the multilayered architecture of that niche in microsatellite-stable (MSS) CRC liver metastases. There, a physical barrier of $SPP1^+$ TAMs and dense extracellular matrix, a chemical exclusion field of CAF-derived CXCL12, and a functionally exhausted environment maintained by $FOLR2^+$ TAMs act together.

Collectively, the evidence indicates that CRC metastasis is not an autonomous, linear evolution of tumor cells, but the outcome of highly coordinated spatiotemporal co-evolution between tumor cells and their microenvironment.

Although these mechanisms are becoming clearer, clinical implementation of combination immunotherapies targeting the microenvironment still faces three obstacles, namely pathway compensation and redundancy, cumulative toxicity, and the absence of predictive biomarkers. The axes described above do not operate in isolation, so interrupting SPP1-CD44 or CXCL12-CXCR4 signaling leaves MIF-CD74 and TGF-β inputs intact, and the malignant cell survives the loss of any single axis. Toxicity compounds the problem, because immune-related adverse events are added to the gastrointestinal, hepatic and hematological toxicity of the cytotoxic or targeted partner, and a combination that is tolerable in a dose-finding study may not be deliverable at the dose intensity that showed activity preclinically. Finally, no marker identifies which pathway dominates in a given tumor, so combinations are still tested in patients selected for MSS status alone, where even a mechanistically sound regimen may fail. A rational combination therefore requires a defined mechanism, a companion biomarker and a randomized design with survival rather than response endpoints.

5. Future Prospects

Despite this progress, translating these discoveries into clinical benefit remains challenging. Major barriers include high technical costs, complex workflows, heavy dependence of data analysis on specialized expertise, and the difficulty of selecting simple, reliable, and clinically validated biomarkers from high-dimensional datasets. The central problem is no longer a lack of data, but how to convert complex biological insights into accessible and efficient clinical tools. Future progress in this field will depend mainly on several priorities.

First, interpretable artificial-intelligence algorithms should be developed to reduce high-dimensional single-cell features into immunohistochemical or digital-pathology scoring systems that can be implemented in routine pathology practice, for example, converting the spatial distribution of $SPP1^+$ TAMs into a reproducible pathological score. Second, spatial multi-omics assays should become more standardized, automated, and affordable so that they can be incorporated into large prospective clinical-trial cohorts. Third, prospective clinical trials should rigorously test whether biomarkers or classification systems based on these technologies can ultimately guide treatment decisions and improve patient survival. Only by successfully crossing this translational gap can the transformative potential of these technologies directly benefit patients.

Author Contributions: Investigation, X.T., C.Z. and H.Y.; writing—original draft preparation, X.T. and C.Z.; writing—review and editing, H.Y.; visualization, X.T., C.Z. and Q.W.; supervision, H.Y. and J.Y.; funding acquisition, H.Y. All authors have read and agreed to the published version of the manuscript.

Funding: This research was funded by the Natural Science Foundation of Hubei Province, grant number 2025AFB684; Health Science and Technology Project of Hubei Provincial Health Commission, grant number WJ2025M178; the 6th Round of Youth Key Talents Project of Renmin Hospital of Wuhan University, grant number RMQNZD2024046.

Institutional Review Board Statement: Not applicable.

Informed Consent Statement: Not applicable.

Data Availability Statement: No new data were created or analyzed in this study. Data sharing is not applicable to this article.

Acknowledgments: During the preparation of this manuscript/study, the authors used PicDoc AI to generate the schematic in Figure 2. All other figures were created with BioRender.com. The authors have reviewed and edited the output and take full responsibility for the content of this publication.

Conflicts of Interest: The authors declare no conflicts of interest.

Abbreviations

The following abbreviations are used in this manuscript:

CAF	cancer-associated fibroblast
cDNA	complementary DNA
CiPDO	chemically induced patient-derived organoid
CRC	colorectal cancer
CRLM	colorectal liver metastases
CRPM	colorectal peritoneal metastases
CSC	cancer stem cell
CTC	circulating tumor cell
CyTOF	cytometry by time-of-flight
ECM	extracellular matrix
EMT	epithelial–mesenchymal transition
EV	extracellular vesicle
FFPE	formalin-fixed, paraffin-embedded
GEM	gel bead in emulsion
MAPK	mitogen-activated protein kinase
MERFISH	multiplexed error-robust fluorescence in situ hybridization
MSS	microsatellite stable
myCAF	myofibroblast-like cancer-associated fibroblast
NGS	next-generation sequencing
NK	natural killer cell
OnFS	oncofetal state
PCR	polymerase chain reaction
pEMT	partial epithelial–mesenchymal transition
PMS	premetastatic state
RT	reverse transcription
SASP	senescence-associated secretory phenotype
scRNA-seq	single-cell RNA sequencing
scWES	single-cell whole-exome sequencing
SMI	single-molecule imaging
spFBA	spatial flux-balance analysis
ST	spatial transcriptomics
TAM	tumor-associated macrophage
TCGA	The Cancer Genome Atlas
TdT	terminal deoxynucleotidyl transferase
TGF-β	transforming growth factor beta
TME	tumor microenvironment
Tn5	Tn5 transposase
TS	template switching
TSO	template-switching oligonucleotide
UMI	unique molecular identifier
VEGFR	vascular endothelial growth factor receptor

References

1. Matsuda, T.; Fujimoto, A.; Igarashi, Y. Colorectal Cancer: Epidemiology, Risk Factors, and Public Health Strategies. *Digestion* **2025**, *106*, 91–99. [CrossRef] [PubMed]
2. Sun, F.; Li, H.; Sun, D.; Fu, S.; Gu, L.; Shao, X.; Wang, Q.; Dong, X.; Duan, B.; Xing, F.; et al. Single-cell omics: Experimental workflow, data analyses and applications. *Sci. China (Life Sci.)* **2025**, *68*, 5–102. [CrossRef] [PubMed]
3. Yu, X.; Abbas-Aghababazadeh, F.; Chen, Y.A.; Fridley, B.L. *Statistical and Bioinformatics Analysis of Data from Bulk and Single-Cell RNA Sequencing Experiments*; Springer Nature: Berlin/Heidelberg, Germany, 2021; pp. 143–175. [CrossRef] [PubMed]
4. Li, L.; Xiong, F.; Wang, Y.; Zhang, S.; Gong, Z.; Li, X.; He, Y.; Shi, L.; Wang, F.; Liao, Q.; et al. What are the applications of single-cell RNA sequencing in cancer research: A systematic review. *J. Exp. Clin. Cancer Res.* **2021**, *40*, 163. [CrossRef] [PubMed]
5. Chen, A.; Kroehling, L.; Ennis, C.S.; Denis, G.V.; Monti, S. A highly resolvedintegrated transcriptomic atlas of human breast cancers. *bioRxiv* **2025**. Update in *NARGenom Bioinform.* **2026**, *8*, lqaf217. https://doi.org/10.1093/nargab/lqaf217. [CrossRef]
6. Lähnemann, D.; Köster, J.; Szczurek, E.; McCarthy, D.J.; Hicks, S.C.; Robinson, M.D.; Vallejos, C.A.; Campbell, K.R.; Beerenwinkel, N.; Mahfouz, A.; et al. Eleven grand challenges in single-cell data science. *Genome Biol.* **2020**, *21*, 31. [CrossRef] [PubMed]
7. Cilento, M.A.; Sweeney, C.J.; Butler, L.M. Spatial transcriptomics in cancer research and potential clinical impact: A narrative review. *J. Cancer Res. Clin. Oncol.* **2024**, *150*, 296. [CrossRef] [PubMed]
8. Ståhl, P.L.; Salmén, F.; Vickovic, S.; Lundmark, A.; Navarro, J.F.; Magnusson, J.; Giacomello, S.; Asp, M.; Westholm, J.O.; Huss, M.; et al. Visualization and analysis of gene expression in tissue sections by spatial transcriptomics. *Science* **2016**, *353*, 78–82. [CrossRef] [PubMed]
9. Kleshchevnikov, V.; Shmatko, A.; Dann, E.; Aivazidis, A.; King, H.W.; Li, T.; Elmentaite, R.; Lomakin, A.; Kedlian, V.; Gayoso, A.; et al. Cell2location maps fine-grained cell types in spatial transcriptomics. *Nat. Biotechnol.* **2022**, *40*, 661–671. [CrossRef] [PubMed]
10. Jovic, D.; Liang, X.; Zeng, H.; Lin, L.; Xu, F.; Luo, Y. Single-cell RNA sequencing technologies and applications: A brief overview. *Clin. Transl. Med.* **2022**, *12*, e694. [CrossRef] [PubMed]
11. Wang, S.; Sun, S.-T.; Zhang, X.-Y.; Ding, H.-R.; Yuan, Y.; He, J.-J.; Wang, M.-S.; Yang, B.; Li, Y.-B. The Evolution of Single-Cell RNA Sequencing Technology and Application: Progress and Perspectives. *Int. J. Mol. Sci.* **2023**, *24*, 2943. [CrossRef] [PubMed]
12. Jinhong, K. Single-Cell RNA Sequencing Analysis Using Fluidigm C1 Platform for Characterization of Heterogeneous Transcriptomes. *Methods Mol. Biol.* **2022**, 2508261–2508278.
13. Ttoouli, D.; Hoffmann, D. Multiplets in scRNA-seq data: Extent of the problem and efficacy of methods for removal. *PLoS ONE* **2025**, *20*, e0333687. [CrossRef] [PubMed]
14. DeLaughter, D.M. The Use of the Fluidigm C1 for RNA Expression Analyses of Single Cells. *Curr. Protoc. Mol. Biol.* **2018**, *122*, e55. [CrossRef] [PubMed]
15. Danielski, K. Guidance on Processing the 10x Genomics Single Cell Gene Expression Assay. In *Single Cell Transcriptomics*; Springer Nature: Berlin/Heidelberg, Germany, 2022; pp. 1–28. [CrossRef] [PubMed]
16. Kraus, G.; Weigelt, M.; Reinhardt, S.; Petzold, A.; Dahl, A.; Bonifacio, E. Reproducibility of 10x Genomics single cell RNA sequencing method in the immune cell environment. *J. Immunol. Methods* **2022**, *502*, 113227. [CrossRef] [PubMed]
17. Slovin, S.; Carissimo, A.; Panariello, F.; Grimaldi, A.; Bouché, V.; Gambardella, G.; Cacchiarelli, D. Single-Cell RNA Sequencing Analysis: A Step-by-Step Overview. In *RNA Bioinformatics*; Springer Nature: Berlin/Heidelberg, Germany, 2021; pp. 343–365. [CrossRef] [PubMed]
18. Tang, D.T.P.; Plessy, C.; Salimullah, M.; Suzuki, A.M.; Calligaris, R.; Gustincich, S.; Carninci, P. Suppression of artifacts and barcode bias in high-throughput transcriptome analyses utilizing template switching. *Nucleic Acids Res.* **2012**, *41*, e44. [CrossRef] [PubMed]
19. Hahaut, V.; Picelli, S. Full-Length Single-Cell RNA-Sequencing with FLASH-seq. In *Single Cell Transcriptomics*; Springer Nature: Berlin/Heidelberg, Germany, 2022; pp. 123–164. [CrossRef] [PubMed]
20. Shi, Z.-X.; Chen, Z.-C.; Zhong, J.-Y.; Hu, K.-H.; Zheng, Y.-F.; Chen, Y.; Xie, S.-Q.; Bo, X.-C.; Luo, F.; Tang, C.; et al. High-throughput and high-accuracy single-cell RNA isoform analysis using PacBio circular consensus sequencing. *Nat. Commun.* **2023**, *14*, 2631. [CrossRef] [PubMed]
21. Jiang, W.; Zhang, X.; Xu, Z.; Cheng, Q.; Li, X.; Zhu, Y.; Lu, F.; Dong, L.; Zeng, L.; Zhong, W.; et al. High-Throughput Single-Nucleus RNA Profiling of Minimal Puncture FFPE Samples Reveals Spatiotemporal Heterogeneity of Cancer. *Adv. Sci.* **2024**, *12*, e2410713. [CrossRef] [PubMed]
22. Xu, Z.; Chen, L.; Lin, X.; Lyu, Y.; Zhou, M.; Chen, H.; Zhang, H.; Zhang, T.; Chen, Y.; Suo, Y.; et al. Single Nucleus Total RNA Sequencing of Formalin-Fixed Paraffin-Embedded Gliomas. *Small Methods* **2024**, *8*, 2301801. [CrossRef] [PubMed]
23. Luo, Q.; Zhang, H. Emergence of Bias During the Synthesis and Amplification of cDNA for scRNA-seq. In *Single Cell Transcriptomics*; Springer Nature: Berlin/Heidelberg, Germany, 2018; pp. 149–158. [CrossRef] [PubMed]
24. Xiang, L.; Rao, J.; Yuan, J.; Xie, T.; Yan, H. Single-Cell RNA-Sequencing: Opening New Horizons for Breast Cancer Research. *Int. J. Mol. Sci.* **2024**, *25*, 9482. [CrossRef] [PubMed]

25. Sasagawa, Y.; Danno, H.; Takada, H.; Ebisawa, M.; Tanaka, K.; Hayashi, T.; Kurisaki, A.; Nikaido, I. Quartz-Seq2: A high-throughput single-cell RNA-sequencing method that effectively uses limited sequence reads. *Genome Biol.* **2018**, *19*, 29. [CrossRef] [PubMed]
26. Lyu, J.; Chen, C. LAST-seq: Single-cell RNA sequencing by direct amplification of single-stranded RNA without prior reverse transcription and second-strand synthesis. *Genome Biol.* **2023**, *24*, 184. [CrossRef] [PubMed]
27. Hagemann-Jensen, M.; Ziegenhain, C.; Sandberg, R. Scalable single-cell RNA sequencing from full transcripts with Smart-seq3xpress. *Nat. Biotechnol.* **2022**, *40*, 1452–1457. [CrossRef] [PubMed]
28. Luo, H.; Hussain, A.; Abbas, M.; Yuan, L.; Shen, Y.; Zhang, Z.; Sun, G.; Yin, X.; Huang, S. Droplet-based single-cell RNA sequencing: Decoding cellular heterogeneity for breakthroughs in cancer, reproduction, and beyond. *J. Transl. Med.* **2025**, *23*, 1091. [CrossRef] [PubMed]
29. Fanli, M. Single-Cell 3′ mRNA Sequencing with 10× Chromium Gel Beads-in-Emulsion (GEM) Kits. In *Immune Mediators in Cancer*; Springer Nature: Berlin/Heidelberg, Germany, 2026; pp. 473–492. [CrossRef] [PubMed]
30. Rafi, F.R.; Heya, N.R.; Hafiz, M.S.; Jim, J.R.; Kabir, M.M.; Mridha, M.F. A systematic review of single-cell RNA sequencing applications and innovations. *Comput Biol. Chem.* **2025**, *115*, 108362. [CrossRef] [PubMed]
31. Meyer, M.; Kircher, M. Illumina Sequencing Library Preparation for Highly Multiplexed Target Capture and Sequencing. *Cold Spring Harb. Protoc.* **2010**, *2010*, pdb.prot5448. [CrossRef] [PubMed]
32. Xie, S.; Leung, A.W.-S.; Zheng, Z.; Zhang, D.; Xiao, C.; Luo, R.; Luo, M.; Zhang, S. Applications and potentials of nanopore sequencing in the (epi)genome and (epi)transcriptome era. *Innov.* **2021**, *2*, 100153. [CrossRef] [PubMed]
33. Wang, B.; Jia, P.; Gao, S.; Zhao, H.; Zheng, G.; Xu, L.; Ye, K. Long and Accurate: How HiFi Sequencing is Transforming Genomics. *Genom. Proteom. Bioinform.* **2025**, *23*, qzaf003. [CrossRef] [PubMed]
34. Wissel, D.; Mehlferber, M.M.; Nguyen, K.M.; Pavelko, V.; Tseng, E.; Robinson, M.D.; Sheynkman, G.M. A systematic benchmark of high-accuracy PacBio long-read RNA sequencing for transcript-level quantification. *Genome Biol.* **2026**, *27*, 110. [CrossRef] [PubMed]
35. Salas, S.M.; Kuemmerle, L.B.; Mattsson-Langseth, C.; Tismeyer, S.; Avenel, C.; Hu, T.; Rehman, H.; Grillo, M.; Czarnewski, P.; Helgadottir, S.; et al. Optimizing Xenium In Situ data utility by quality assessment and best-practice analysis workflows. *Nat. Methods* **2025**, *22*, 813–823. [CrossRef] [PubMed]
36. Chen, K.H.; Boettiger, A.N.; Moffitt, J.R.; Wang, S.; Zhuang, X. RNA imaging. Spatially resolved, highly multiplexed RNA profiling in single cells. *Science* **2015**, *348*, aaa6090. [CrossRef] [PubMed]
37. He, L.; Dang, K.; Sun, Q.; Wang, W.; Li, W.; Zhang, W.; Ye, K.; Wang, H.; Li, Z.; Guo, Y.; et al. High-Resolution Multiplexed Sequencing of Single-Cell Full-length Transcriptome Via Combinational Barcoded Tn5 Transposon Insertion. *Adv. Sci.* **2025**, *13*, e16013. [CrossRef] [PubMed]
38. Li, Y.; Huang, Z.; Xu, L.; Fan, Y.; Ping, J.; Li, G.; Chen, Y.; Yu, C.; Wang, Q.; Song, T.; et al. UDA-seq: Universal droplet microfluidics-based combinatorial indexing for massive-scale multimodal single-cell sequencing. *Nat. Methods* **2025**, *22*, 1199–1212. [CrossRef] [PubMed]
39. Rao, A.; Barkley, D.; França, G.S.; Yanai, I. Exploring tissue architecture using spatial transcriptomics. *Nature* **2021**, *596*, 211–220. [CrossRef] [PubMed]
40. Williams, C.G.; Lee, H.J.; Asatsuma, T.; Vento-Tormo, R.; Haque, A. An introduction to spatial transcriptomics for biomedical research. *Genome Med.* **2022**, *14*, 68. [CrossRef] [PubMed]
41. Du, M.R.M.; Wang, C.; Law, C.W.; Amann-Zalcenstein, D.; Anttila, C.J.A.; Ling, L.; Hickey, P.F.; Sargeant, C.J.; Chen, Y.; Ioannidis, L.J.; et al. Benchmarking spatial transcriptomics technologies with the multi-sample SpatialBenchVisium dataset. *Genome Biol.* **2025**, *26*, 77. [CrossRef] [PubMed]
42. Chen, A.; Liao, S.; Cheng, M.; Ma, K.; Wu, L.; Lai, Y.; Qiu, X.; Yang, J.; Xu, J.; Hao, S.; et al. Spatiotemporal transcriptomic atlas of mouse organogenesis using DNA nanoball-patterned arrays. *Cell* **2022**, *185*, 1777–1792.e21. [CrossRef] [PubMed]
43. Nagendran, M.; Sapida, J.; Arthur, J.; Yin, Y.; Tuncer, S.D.; Anaparthy, N.; Gupta, A.; Serra, M.; Patterson, D.; Tentori, A. 1457 Visium HD enables spatially resolved, single-cell scale resolution mapping of FFPE human breast cancer tissue. *J. Immunother. Cancer* **2023**, *11*, A1620. [CrossRef]
44. Stickels, R.R.; Murray, E.; Kumar, P.; Li, J.; Marshall, J.L.; Di Bella, D.J.; Arlotta, P.; Macosko, E.Z.; Chen, F. Highly sensitive spatial transcriptomics at near-cellular resolution with Slide-seqV2. *Nat. Biotechnol.* **2020**, *39*, 313–319. [CrossRef] [PubMed]
45. Janesick, A.; Shelansky, R.; Gottscho, A.D.; Wagner, F.; Williams, S.R.; Rouault, M.; Beliakoff, G.; Morrison, C.A.; Oliveira, M.F.; Sicherman, J.T.; et al. High-resolution mapping of the tumor microenvironment using integrated single-cell, spatial, and in situ analysis. *Nat. Commun.* **2023**, *14*, 8353. [CrossRef] [PubMed]
46. Tian, L.; Chen, F.; Macosko, E.Z. The expanding vistas of spatial transcriptomics. *Nat. Biotechnol.* **2022**, *41*, 773–782. [CrossRef] [PubMed]

47. Chen, H.; Chen, Y.-S.; Zhang, S.; Chen, J.; Yang, H.; Fan, T.; Zheng, J.; Liao, Y.; Liang, Q.; Wang, Y. Automated in situ microfluidic Random-seq for robust single-nucleus and spatial total RNA profiling of diverse FFPE specimens. *Nat. Commun.* **2026**, *17*, 8282. [CrossRef] [PubMed]
48. Zhao, Y.; Li, Y.; He, Y.; Wu, J.; Liu, Y.; Li, X.; Li, Z.; Yuan, Q.; Li, J.; Zhang, X.; et al. Stereo-seq V2: Spatial mapping of total RNA on FFPE sections with high resolution. *Cell* **2025**, *188*, 6554–6571.e21. [CrossRef] [PubMed]
49. Lee, J.Y.; Kannan, B.; Neo, Z.W.; Rajasegaran, V.; Lim, J.C.T.; Yeong, J.P.S.; Chan, J.Y. A Protocol for Spatial Transcriptomics Using the 10× Genomics Visium Platform. In *Cellular Spatial Characterization and Analysis*; Springer Nature: Berlin/Heidelberg, Germany, 2026; pp. 151–217. [CrossRef] [PubMed]
50. Ma, Y.; Zhou, X. Spatially informed cell-type deconvolution for spatial transcriptomics. *Nat. Biotechnol.* **2022**, *40*, 1349–1359. [CrossRef] [PubMed]
51. Lin, K.; Chowdhury, S.; Zeineddine, M.A.; Zeineddine, F.A.; Hornstein, N.J.; Villarreal, O.E.; Maru, D.M.; Haymaker, C.L.; Vauthey, J.-N.; Chang, G.J.; et al. Identification of Colorectal Cancer Cell Stemness from Single-Cell RNA Sequencing. *Mol. Cancer Res.* **2023**, *22*, 337–346. [CrossRef] [PubMed]
52. Li, R.; Liu, X.; Huang, X.; Zhang, D.; Chen, Z.; Zhang, J.; Bai, R.; Zhang, S.; Zhao, H.; Xu, Z.; et al. Single-cell transcriptomic analysis deciphers heterogenous cancer stem-like cells in colorectal cancer and their organ-specific metastasis. *Gut* **2023**, *73*, 470–484. [CrossRef] [PubMed]
53. Zhan, Y.; Sun, D.; Gao, J.; Gao, Q.; Lv, Y.; Du, T.; Dong, Y.; Wang, Y.; Zhan, H.; Li, J.; et al. Single-cell transcriptomics reveals intratumor heterogeneity and the potential roles of cancer stem cells and myCAFs in colorectal cancer liver metastasis and recurrence. *Cancer Lett.* **2025**, *612*, 217452. [CrossRef] [PubMed]
54. Alvarez-Villanueva, D.; Maqueda, M.; Harti, D.; Canton, E.; Andrades, E.; Bertran, J.; Martínez-Iniesta, M.; Solé, L.; García-Hernández, V.; Montoto, Á.; et al. Tight junction-high and CDH17-positive cell population is the source of colorectal cancer liver metastases. *Nat. Commun.* **2026**, *17*, 1425. [CrossRef] [PubMed]
55. Pan, Y.; Xiang, X.; Li, J.; Ge, Y.; Liang, X. Single-cell transcriptome analysis reveals SOX9 mutation-driven tumor stemness and microenvironment remodeling through the COL1A1–CD44 axis in colorectal cancer. *BMC Cancer* **2026**, *26*, 921. [CrossRef] [PubMed]
56. Yu, C.; Lu, W.; Wu, J.; Fang, X.; Wang, X.; Zhang, G.; Chen, S.; Mei, Y.; Chen, H.; Ye, F.; et al. Liver metastasis or peritoneal metastasis: Single-cell RNA sequencing reveals the organotropism in colorectal cancer is driven by distinct partial-EMT processes. *Cancer Lett.* **2025**, *629*, 217880. [CrossRef] [PubMed]
57. Ning, W.; Jia, W.; Ning, J.; Zhou, L.; Li, Z.; Zhang, L.; Song, X. Cross-cohort multi-omics analysis identifies novel clusters driven by EMT signatures in colorectal cancer. *Front. Immunol.* **2025**, *16*, 1628005. [CrossRef] [PubMed]
58. Tang, J.; Chen, Z.; Zhang, D.; Jin, K.; Xu, H.; Tian, C.; Duan, J.; Yang, S.; Sun, Q.; Feng, Y.; et al. ENO2 drives tumor cell-induced M2 macrophage polarization to promote colorectal cancer liver metastasis. *Signal Transduct. Target. Ther.* **2026**, *11*, 166. [CrossRef] [PubMed]
59. Song, C.; Sun, H.; Gan, W.; Liu, Q.; Wu, L.; Zhu, M.; Zhu, L. APOE+ macrophages induce tumor cell metastatic characteristics via TNFSF12/TNFRSF12A signaling, correlating with poor patient prognosis. *Cancer Cell Int.* **2026**, *26*, 261. [CrossRef] [PubMed]
60. Yang, S.; Zhang, D.; Sun, Q.; Nie, H.; Zhang, Y.; Wang, X.; Huang, Y.; Sun, Y. Single-Cell and Spatial Transcriptome Profiling Identifies the Transcription Factor BHLHE40 as a Driver of EMT in Metastatic Colorectal Cancer. *Cancer Res.* **2024**, *84*, 2202–2217. [CrossRef] [PubMed]
61. Lu, Y.; Chen, Y.; Wang, Z.; Shen, H.; Xu, L.; Huang, C.; Tong, Y.; Shao, Y.; Zhang, H.; Fu, Z. Single-cell and spatial transcriptome profiling reveal CTHRC1+ fibroblasts promote EMT through WNT5A signaling in colorectal cancer. *J. Transl. Med.* **2025**, *23*, 282. [CrossRef] [PubMed]
62. Zhou, X.; Han, J.; Zuo, A.; Ba, Y.; Liu, S.; Xu, H.; Zhang, Y.; Weng, S.; Zhou, Z.; Liu, L.; et al. THBS2 + cancer-associated fibroblasts promote EMT leading to oxaliplatin resistance via COL8A1-mediated PI3K/AKT activation in colorectal cancer. *Mol. Cancer* **2024**, *23*, 282. [CrossRef] [PubMed]
63. Yang, F.; Li, Y.; Shang, X.; Zhu, Y.; Hou, W.; Liu, Y.; Hua, Q.; Sun, Z. PLIN2 promotes colorectal cancer progression through CD36-mediated epithelial-mesenchymal transition. *Cell Death Dis.* **2025**, *16*, 510. [CrossRef] [PubMed]
64. Cammareri, P.; Raponi, M.; Hong, Y.; Billard, C.V.; Peckett, N.; Zhu, Y.; Velez-Bravo, F.D.; Younger, N.T.; Dunican, D.S.; Pohl, S.Ö.-G.; et al. Loss of colonic fidelity enables multilineage plasticity and metastasis. *Nature* **2025**, *644*, 547–556. [CrossRef] [PubMed]
65. Xiong, L.; Xu, Y.; Gao, Z.; Shi, J.; Wang, Y.; Wang, X.; Huang, W.; Li, M.; Wang, L.; Xu, J.; et al. A patient-derived organoid model captures fetal-like plasticity in colorectal cancer. *Cell Res.* **2025**, *35*, 642–655. [CrossRef] [PubMed]
66. Fang, X.; Huang, H.; Zhao, Z.; Yang, L.; Huang, F.; Li, J.; Meng, Z.; He, S.; Li, T.; Yang, S.; et al. KLF7 as a biomarker for the pre-metastatic state promotes colorectal cancer liver metastasis via TGFβ autocrine signaling. *Cancer Lett.* **2026**, *639*, 218123. [CrossRef] [PubMed]

67. Ma, Y.; Wang, L.; Zhang, Z.; Zhao, Y.; Zhao, Z.; Luo, R.; Wang, J.; Guo, L.; Fu, W.; Miao, K.; et al. Comprehensive single-cell transcriptome landscape of metastatic colorectal cancer identifies budding-potential cells and their interactions with cancer-associated fibroblasts. *npj Precis. Oncol.* **2025**, *9*, 408. [CrossRef] [PubMed]
68. Wang, J.; He, Q.; Hu, J.; Gao, L.; Sheng, N.; Zhou, S.; Gong, J.; Gu, Y.; Chen, H.; Xu, Y.; et al. A multi-omics dissection of INHBA+ CAF-mediated epithelial-mesenchymal transition and immune suppression in colorectal cancer. *J. Transl. Med.* **2026**, *24*, 885. [CrossRef] [PubMed]
69. Wu, S.; Zhang, G.; Yang, J.; Wang, S. The Single-Cell and Spatial Transcriptomics Atlas of Epithelial–Fibroblast Interactions in Colorectal Cancer. *Dig. Dis. Sci.* **2026**, *71*, 4151–4162. [CrossRef] [PubMed]
70. Amorie, J.R.B.D.; Hageman, J.H.; Brunner, S.R.; van der Horst, S.E.M.; Puschhof, M.C.; van Hoeck, A.; van Lierop, I.; Middelkamp, S.; van der Schee, L.; van Kempen, S.; et al. Emergence of oncofetal plasticity is ubiquitous in early colorectal cancers. *Nature* **2026**, *654*, 229–239. [CrossRef] [PubMed]
71. Maspero, D.; Marteletto, G.; Lapi, F.; Galuzzi, B.G.; Ruano, I.; Vandenbosch, B.; Yin, K.; Tejpar, S.; Graudenzi, A.; Heyn, H.; et al. Spatial FBA reveals heterogeneous Warburg niches in renal tumors and lactate consumption in colorectal cancer. *npj Syst. Biol. Appl.* **2026**, *12*, 32. [CrossRef] [PubMed]
72. Singh, T. Spatial Transcriptomics Reveals Stromal-Partitioned Growth in Primary Colorectal Cancer and Host-Permeated Architecture in Liver Metastases. *Preprint* **2026**. [CrossRef] [PubMed]
73. Wang, P.-X.; Zhong, Y.-C.; Zheng, W.-J.; Xian, J.-R.; Song, F.; Xu, J.; Sun, Y.-F.; Cheng, J.-W.; Feng, H.-Y.; Jiang, X.; et al. Multi-omic profiling identifies TREM2+ lipid-laden macrophages as inflammatory drivers and therapeutic targets of colorectal cancer liver metastasis. *Cancer Lett.* **2026**, *656*, 218657. [CrossRef] [PubMed]
74. Bin Lim, S.; Lim, C.T.; Lim, W.-T. Single-Cell Analysis of Circulating Tumor Cells: Why Heterogeneity Matters. *Cancers* **2019**, *11*, 1595. [CrossRef] [PubMed]
75. Kaifi, J.T.; Kunkel, M.; Das, A.; Harouaka, R.A.; Dicker, D.T.; Li, G.; Zhu, J.; Clawson, G.A.; Yang, Z.; Reed, M.F.; et al. Circulating tumor cell isolation during resection of colorectal cancer lung and liver metastases: A prospective trial with different detection techniques. *Cancer Biol. Ther.* **2015**, *16*, 699–708. [CrossRef] [PubMed]
76. Ren, X.; Song, M.; Liu, X.; He, W. Circulating tumor cells: Mechanisms and clinical significance in colorectal cancer metastasis. *Mol. Cancer* **2025**, *24*, 242. [CrossRef] [PubMed]
77. Cai, J.; Zhang, W.; Lu, Y.; Liu, W.; Zhou, H.; Liu, M.; Bi, X.; Liu, J.; Chen, J.; Yin, Y.; et al. Single-cell exome sequencing reveals polyclonal seeding and TRPS1 mutations in colon cancer metastasis. *Signal Transduct. Target. Ther.* **2024**, *9*, 247. [CrossRef] [PubMed]
78. Li, Q.; Xiao, Y.; Han, L.; Luo, W.; Dai, W.; Fang, H.; Wang, R.; Xu, Y.; Cai, S.; Goel, A.; et al. Microbiome dysbiosis, neutrophil recruitment and mesenchymal transition of mesothelial cells promotes peritoneal metastasis of colorectal cancer. *Nat. Cancer* **2025**, *6*, 493–510. [CrossRef] [PubMed]
79. Wang, S.; Ye, G.; Xu, X.; Lin, Y.; Li, X.; Zhang, Z.; Qi, M.; Tan, L.; Cheng, M.; Zhang, H.; et al. Pericyte drives the formation of circulating tumour cell-neutrophil clusters to promote colorectal cancer metastasis. *Gut* **2025**, *75*, 81–93. [CrossRef] [PubMed]
80. Masmoudi, D.; Villalba, M.; Alix-Panabières, C. Natural killer cells: The immune frontline against circulating tumor cells. *J. Exp. Clin. Cancer Res.* **2025**, *44*, 118. [CrossRef] [PubMed]
81. Liu, X.; Song, J.; Zhang, H.; Liu, X.; Zuo, F.; Zhao, Y.; Zhao, Y.; Yin, X.; Guo, X.; Wu, X.; et al. Immune checkpoint HLA-E:CD94-NKG2A mediates evasion of circulating tumor cells from NK cell surveillance. *Cancer Cell* **2023**, *41*, 272–287.e9. [CrossRef] [PubMed]
82. Ding, D.; Li, W.; Ren, J.; Li, Y.; Jiang, G.; Liang, R.; Huang, H.; You, J.; Wang, Y.; Wei, B. SPP1 high macrophage-induced T-cell stress promotes colon cancer liver metastasis through SPP1/CD44/PI3K/AKT signaling. *J. Immunother. Cancer* **2025**, *13*, e012330. [CrossRef] [PubMed]
83. Henriques, A.; Salvany-Celades, M.; Nieto, P.; Palomo-Ponce, S.; Sevillano, M.; Hernando-Momblona, X.; Middendorp-Guerra, E.; Martinez, M.L.; Haak, E.M.; Nieto, J.; et al. TGF-β builds a dual immune barrier in colorectal cancer by impairing T cell recruitment and instructing immunosuppressive SPP1+ macrophages. *Nat. Genet.* **2025**, *57*, 3050–3065. [CrossRef] [PubMed]
84. Cao, J.; Qin, S.; Li, B.; Zhang, Z.; Miao, P.; Yan, H.; Duan, J.; He, B.; He, K.; Peng, P.; et al. Extracellular vesicle-induced lipid dysregulation drives liver premetastatic niche formation in colorectal cancer. *Gut* **2025**, *74*, 2012–2023. [CrossRef] [PubMed]
85. Dai, C.S.; Mishra, A.; Edd, J.; Toner, M.; Maheswaran, S.; Haber, D.A. Circulating tumor cells: Blood-based detection, molecular biology, and clinical applications. *Cancer Cell* **2025**, *43*, 1399–1422. [CrossRef] [PubMed]
86. Liu, Y.; Zhang, Q.; Xing, B.; Luo, N.; Gao, R.; Yu, K.; Hu, X.; Bu, Z.; Peng, J.; Ren, X.; et al. Immune phenotypic linkage between colorectal cancer and liver metastasis. *Cancer Cell* **2022**, *40*, 424–437.e5. [CrossRef] [PubMed]
87. Lin, Y.; Chen, Z.; Zhao, S.; Zhao, L.; Yang, C.; Zhu, M.; Ye, Y.; Wang, S.; Shen, Z. Targeting SPP1 + TAMs associated with liver metastasis reverses immunosuppression and synergizes with immunotherapy in colorectal cancer. *J. Immunother. Cancer* **2026**, *14*, e014128. [CrossRef] [PubMed]

88. Marzano, P.; Soldani, C.; Cazzetta, V.; Franceschini, B.; Terzoli, S.; Carletti, A.; Polidoro, M.A.; Marchesi, F.; Locati, M.; Basso, G.; et al. Tissue-Specific Immunosuppressive and Proliferating Macrophages Fuel Early Metastatic Progression of Human Colorectal Cancer to the Liver. *Cancer Immunol. Res.* **2025**, *13*, 1783–1797. [CrossRef] [PubMed]
89. Xie, S.; Li, J.; Heng, S.; Xiao, J.; Chen, J.; Qi, X. Integrated single-cell and spatial transcriptomics uncover SPP1^{+} and HLA-DRB5^{+} macrophages as key modulators of the immune microenvironment in colorectal cancer liver metastasis. *J. Transl. Med.* **2026**, *24*, 370. [CrossRef] [PubMed]
90. Zhang, F.; Zhao, B.; Fan, X.; Shi, Z.; Guo, P.; Zhang, H.; Kwan, H.-Y.; Liu, Z.; Su, T. CD44/POU2F2/BCL9L axis mediates MIF-driven SPP1^{+} TAM activation in colorectal cancer metastasis. *Int. J. Biol. Sci.* **2026**, *22*, 2492–2511. [CrossRef] [PubMed]
91. García-Rodríguez, J.L.; Korsgaard, U.; Vissing, S.M.; Paasch, T.P.; Semenova, M.; Vendelbo, S.L.; Jensby, E.F.; Williams, H.L.; Salachan, P.V.; Brandt, C.B.; et al. Cancer-associated fibroblasts shape the formation of budding cancer cells at the invasive front of human colorectal cancer. *Commun. Biol.* **2025**, *8*, 1345. [CrossRef] [PubMed]
92. Sathe, A.; Mason, K.; Grimes, S.M.; Zhou, Z.; Lau, B.T.; Bai, X.; Su, A.; Tan, X.; Lee, H.; Suarez, C.J.; et al. Colorectal Cancer Metastases in the Liver Establish Immunosuppressive Spatial Networking between Tumor-Associated SPP1 + Macrophages and Fibroblasts. *Clin. Cancer Res.* **2022**, *29*, 244–260. [CrossRef] [PubMed]
93. Liu, S.; Zhang, Z.; Wang, Z.; Liu, C.; Liang, G.; Xu, T.; Li, Z.; Duan, X.; Xu, G.; Feng, X.; et al. SPP1 Drives Colorectal Cancer Liver Metastasis and Immunotherapy Resistance by Stimulating CXCL12 Production in Cancer-Associated Fibroblasts. *Cancer Res.* **2025**, *86*, 58–79. [CrossRef] [PubMed]
94. Zhang, Y.; Zuo, A.; Ba, Y.; Liu, S.; Chen, J.; Yang, S.; Weng, S.; Chen, Y.; Xu, H.; Luo, P.; et al. Cancer-associated fibroblast-derived SEMA3C facilitates colorectal cancer liver metastasis via NRP2-mediated MAPK activation. *Proc. Natl. Acad. Sci. USA* **2025**, *122*, e2423077122. [CrossRef] [PubMed]
95. Ye, T.; Chen, M.; Hu, Y.; Yang, Z.; Xu, J.; Zhang, Y.; Zhou, S.; Yu, Y.; Chen, Y.; Zhang, Z.; et al. Vesicular QSOX1-MMP2 from inflammatory cancer-associated fibroblasts degrades the extracellular matrix to drive colorectal cancer pulmonary dissemination. *Cancer Lett.* **2026**, *656*, 218645. [CrossRef] [PubMed]
96. Yang, S.; Chen, Y.; Liu, S.; Zuo, A.; Ba, Y.; Zhang, Y.; Liu, B.; Zhang, C.; Xu, H.; Luo, P.; et al. Macrophage-Induced Senescent Cancer-Associated Fibroblasts Promote SASP-Mediated Chemoresistance in Colorectal Cancer. *Cancer Res.* **2026**, *86*, 4772–4791. [CrossRef] [PubMed]
97. Fukumura, D.; Kloepper, J.; Amoozgar, Z.; Duda, D.G.; Jain, R.K. Enhancing cancer immunotherapy using antiangiogenics: Opportunities and challenges. *Nat. Rev. Clin. Oncol.* **2018**, *15*, 325–340. [CrossRef] [PubMed]
98. Gao, Q.; Ling, X.; Liao, L.; Tang, F.; Jiang, Y.; Qin, S.; Hou, W.; Zhou, W.; Jiang, L.; Xiao, C.; et al. Remodeling of T and endothelial cells during total neoadjuvant therapy in rectal cancer. *Cancer Cell* **2025**, *43*, 2282–2297.e9. [CrossRef] [PubMed]
99. Qi, X.; Hou, S.; Xie, S.; Chen, J. Integrative single-cell and spatial transcriptomic analysis reveals lipid metabolism–mediated macrophage heterogeneity during colorectal cancer liver metastasis progression. *J. Transl. Med.* **2025**, *24*, 117. [CrossRef] [PubMed]
100. Zhu, C.; Liu, Y.; Xu, S.; Li, R.; Shi, J.; Tang, G.; Ran, R.; Pang, B.; Chi, Z.; Ding, Y.; et al. Multi-omics reveals CXCR4 drives immune escape in colorectal cancer via metabolic reprogramming and immune microenvironment remodeling. *Cell Death Dis.* **2026**, *17*, 591. [CrossRef] [PubMed]
101. Wang, W.; Deng, Y.; Li, W.; Wang, R.; Zhou, C.; Xu, Y.; He, J.; Liao, L.E.; Lan, J.; Yu, L.; et al. Feedback regulation between histone H3 lysine 18 lactylation and TROP2-mediated glycolysis drives metastatic progression of colorectal cancer. *Clin. Transl. Med.* **2026**, *16*, e70562. [CrossRef] [PubMed]
102. Li, L.; Zhao, L.; Cao, K.; Zhang, P.; Xu, G.; Zheng, J.; Lin, Z.; Yu, D.; Ren, J.; Zhang, J.; et al. Hepatocytes functionally reprogrammed by KIAA1199-high colorectal cancer cells favour the accumulation of pro-metastatic Egr1+ neutrophils. *Nat. Commun.* **2026**, *17*, 2462. [CrossRef] [PubMed]

Disclaimer/Publisher's Note: The statements, opinions and data contained in all publications are solely those of the individual author(s) and contributor(s) and not of MDPI and/or the editor(s). MDPI and/or the editor(s) disclaim responsibility for any injury to people or property resulting from any ideas, methods, instructions or products referred to in the content.